



UNIVERSIDADE D  
COIMBRA

Ana Sofia Cartaxo Pinto Oliveira

**AUTOMATIZING THE APPLICATION OF COLD  
ATMOSPHERIC PLASMA IN TUMOR CELLS**

Dissertação no âmbito do Mestrado Integrado em Engenharia Biomédica orientada pelo Prof Doutor Pedro Mariano Simões Neto e pelo Prof Doutor Francisco José Santiago Fernandes Amado Caramelo e apresentada ao Departamento de Engenharia Mecânica da Faculdade de Ciências e Tecnologia da Universidade de Coimbra.

Setembro de 2019





UNIVERSIDADE D  
**COIMBRA**

Ana Sofia Cartaxo Pinto Oliveira

**AUTOMATIZING THE APPLICATION OF COLD  
ATMOSPHERIC PLASMA IN TUMOR CELLS**

Dissertação no âmbito do Mestrado Integrado em Engenharia Biomédica orientada pelo Prof Doutor Pedro Mariano Simões Neto e pelo Prof Doutor Francisco José Santiago Fernandes Amado Caramelo e apresentada ao Departamento de Engenharia Mecânica da Faculdade de Ciências e Tecnologia da Universidade de Coimbra.

Setembro de 2019



This project was developed in collaboration with:

Collaborative Robotics Laboratory of University of Coimbra



Centre for Innovative Biomedicine and Biotechnology



Coimbra Institute for Clinical and Biomedical Research



Biophysics Institute of the Faculty of Medicine of University of Coimbra



Faculty of Medicine of University of Coimbra, Portugal and Faculty of Science and Technology of University of Coimbra, Portugal

This research was partially supported by Portugal 2020 project DM4Manufacturing POCI-01-0145-FEDER-016418 by UE/FEDER through the program COMPETE 2020, and the Portuguese Foundation for Science and Technology (FCT) COBOTIS (PTDC/EMEEME/ 32595/2017).





Esta cópia da dissertação é fornecida na condição de que quem a consulta reconhece que os direitos de autor são pertença do autor da dissertação e que nenhuma citação ou informação obtida a partir dela pode ser publicada sem a referência apropriada.

This copy of the thesis has been supplied on condition that anyone who consults it is understood to recognize that its copyright rests with its author and that no quotation from the thesis and no information derived from it may be published without proper acknowledgement.





# Agradecimentos

Quero começar por agradecer aos meus orientadores Prof Doutor Pedro Neto do Departamento de Engenharia Mecânica da Faculdade de Ciências e Tecnologia da Universidade de Coimbra, ao Prof Doutor Francisco Caramelo e à Doutora Mafalda Laranjo do Instituto de Biofísica da Faculdade de Medicina da Universidade de Coimbra pelo enorme apoio, simpatia, ajuda e disponibilidade ao longo do projeto. Obrigada por me terem incentivado para fazer sempre melhor, por todas as críticas e conselhos para tornar este projeto possível!

Aos meus colegas de laboratório do Departamento de Engenharia Mecânica da Universidade de Coimbra, por todo o apoio ao longo do meu projeto. Obrigada por todas as dicas e críticas, e obrigada pela boa disposição sempre presente! Quero, também, agradecer a todos os colegas do Instituto de Biofísica da Faculdade de Medicina da Universidade de Coimbra pela disponibilidade e ajuda constante, por todas as dicas e apoio que, direta ou indiretamente, contribuíram para o projeto.

A todos os meus amigos, quero agradecer profundamente pelo carinho e amizade. Obrigada por não se esquecerem de mim e me apoiarem mesmo quando eu estou mais ausente.

À minha família, pelo amor incondicional e por acreditarem sempre em mim. Mãe e Pai, obrigada por me fazerem sonhar sempre mais alto e me apoiarem sempre em todas as minhas decisões!



“If I had only one hour to save the world, I would spend fifty-five minutes defining the problem, and only five minutes finding the solution.”

-Albert Einstein



# Abstract

In the medical research field, a relevant part of the time that researchers spend in the laboratory is doing repetitive tasks that are highly time-consuming and prone to errors. Automatization of laboratory techniques and procedures is important to make the time of the researchers more profitable and focused on high value-added investigation tasks. The replacement of human labour by automatized labour can also avoid possible human errors in the procedures, making the processes more efficient and rigorous.

At the Coimbra Institute for Clinical and Biomedical Research (iCBR), at the Biophysics Institute of the Faculty of Medicine of the University of Coimbra, Cold Atmospheric Plasma (CAP) is being applied in tumor cell lines to study its properties in cancer treatment, namely the tumor cell lines of endometrium. The application of CAP to culture cells, in the compartments of multiwell plates, is a repetitive and time-consuming technique, performed using a completely manual system.

The main focus of the present thesis was to fully automatize the laboratory technique of CAP application in cell lines.

The automatization of the technique consisted on the development of a linear robot capable of autonomously performing the application of CAP to cells, without human intervention, in order to increase the rentability of researchers' time in the laboratory and improve the reproductivity of the experiments.

A cartesian robot was developed according to the requirements and, then, several tests for the validation of the robotic system were performed.

The executed tests consisted on applying CAP to three different cell lines of endometrial cancer and, afterwards, performing viability assays to evaluate cell viability after the exposure to CAP. CAP irradiation was performed manually and, posteriorly, with the robotic system, in order to compare the results and conclude about the use of the robotic system in this research.

Obtained results showed that, with the use of the robotic system, the duration of the technique of CAP irradiation of cell lines is reduced to half, in an autonomous way,

which suggests that the researchers' work in the laboratory can be more efficient with the support of the robotic system.

Furthermore, this thesis demonstrated that the use of the robotic system to perform CAP irradiation in cell lines reduces the variability of results without interfering with the influence of CAP properties regarding cells, which means that the robotic system is more precise for the application of CAP than the manual system.

In terms of biological analysis, the cell viability decreased in response to the increase of time exposure to CAP, which demonstrates the potential of CAP in cancer treatment. The achieved results promote further research to understand CAP mechanisms for *in vivo* studies.

It was also possible to encourage the development of robotic solutions in medical laboratory research and in other clinical applications. Human-Robot interaction can become an advantageous synergy since researchers' time becomes more profitable and automated tasks can be performed more accurately.

**Key words:** Robotics, Cold Atmospheric Plasma, Endometrial Cancer, Human-Robot interaction, Automatizing.

# Resumo

Na área da investigação médica, uma parcela relevante do tempo que os investigadores passam no laboratório é a realizar tarefas repetitivas que consomem muito tempo e são propensas a erros. A automatização de técnicas e procedimentos de laboratório é importante de modo tornar o tempo dos investigadores mais rentável e centrado em tarefas de investigação de alto valor agregado. A substituição do trabalho humano por trabalho automatizado também pode evitar possíveis erros humanos nos procedimentos, tornando, assim, os processos mais eficientes e rigorosos.

No iCBR, no Instituto de Biofísica da Faculdade de Medicina da Universidade de Coimbra, o Plasma Frio Atmosférico (PFA) tem vindo a ser aplicado em linhas celulares tumorais para estudar as suas propriedades no tratamento do cancro. A aplicação de PFA em cultura de células, é realizada nos compartimentos de placas de múltiplos poços. Caracteriza-se por ser uma técnica repetitiva e demorada, realizada usando um sistema totalmente manual.

O principal foco da presente tese foi a automatização completa da técnica laboratorial de aplicação de PFA em linhas celulares.

A automatização da técnica consistiu no desenvolvimento de um robot linear capaz de realizar autonomamente a aplicação do PFA em células sem intervenção humana, a fim de aumentar a rentabilidade do tempo dos investigadores nos laboratórios e bem como a reprodutividade das experiências.

Foi desenvolvido um robot cartesiano de acordo com todos os requisitos necessários para a sua aplicação e, posteriormente, foram realizados testes para a validação do sistema robótico. Os testes realizados consistiram na aplicação de PFA em três linhas celulares tumorais de endométrio e, seguidamente, foram realizados ensaios de viabilidade para avaliar a viabilidade celular após a exposição das células ao PFA. A irradiação com PFA foi realizada manualmente e, posteriormente, com o sistema robótico desenvolvido para poder comparar os resultados e concluir sobre o uso e influência do sistema robótico neste tipo de estudo.

Os resultados obtidos mostraram que, com o uso do sistema robótico, o tempo de irradiação com PFA das linhas celulares é reduzido para metade, permitindo a sua

realização de forma autónoma, o que sugere que o trabalho dos investigadores no laboratório pode tornar-se mais produtivo. O tempo dos investigadores em laboratório pode, assim, tornar-se mais lucrativo e rentável com o apoio do sistema robótico na realização desta técnica. Além disso, este trabalho demonstrou que o uso deste sistema robótico, para realizar a irradiação com PFA de linhas celulares, aparenta reduzir a variabilidade dos resultados sem interferir na influência das propriedades do PFA sobre as células, o que sugere que este sistema robótico seja mais preciso na aplicação de PFA do que a realização manual da tarefa.

Em termos de análise biológica, a viabilidade celular diminuiu em resposta ao aumento do tempo de exposição celular ao PFA, o que demonstra o potencial do PFA no tratamento do cancro. Portanto, os resultados obtidos encorajam um aprofundamento na investigação de modo a entender os mecanismos do PFA para estudos *in vivo*.

Foi ainda possível incentivar o desenvolvimento de soluções robóticas a nível da investigação laboratorial médica e possíveis aplicações clínicas. A interação Humano-Robot pode tornar-se numa sinergia bastante vantajosa, na medida em que o tempo dos profissionais se pode tornar mais rentável e as tarefas automatizadas serem realizadas com maior precisão.

**Palavras-chave:** Robótica, Plasma Frio Atmosférico, Cancro do Endométrio, Interação Homem-Robot, Automatização.



# Table of Contents

Agradecimientos .....	i
Abstract .....	v
Resumo.....	vii
Table of Contents .....	ix
List of Figures.....	xi
List of Tables .....	xiii
List of Abbreviations.....	xiv
<b>Chapter 1: Introduction.....</b>	<b>1</b>
1.1 Problem and Motivation .....	2
1.2 Proposed Approach .....	2
1.3 Thesis Overview.....	3
<b>Chapter 2: Literature Review.....</b>	<b>4</b>
2.1 Endometrial Cancer .....	5
2.1.1 Therapies in Endometrial Cancer Treatments .....	9
2.2 Cold Atmospheric Plasma .....	10
2.2.1 Characteristics of Cold Atmospheric Plasma .....	10
2.2.2 Application of Plasma in Medicine.....	11
2.2.3 Cold Atmospheric Plasma in Cancer Treatment.....	12
2.2.4 System of Application of Cold Atmospheric Plasma.....	13
2.3 Robotic-Based Solutions .....	15
2.3.1 Robots in Biomedical Research .....	16
<b>Chapter 3: Robotic System .....</b>	<b>19</b>
3.1 Requirements.....	19
3.1.1 Functional Requirements.....	19
3.1.2 Non-Functional Requirements.....	22
3.2 Robotic Mechanism .....	23

3.3	End-Effector .....	26
<b>Chapter 4: Human-Machine Interface.....</b>		<b>33</b>
4.1	Graphical User Interface .....	33
4.2	Numerical Control .....	36
4.2.1	G-Code.....	37
<b>Chapter 5: Procedures.....</b>		<b>43</b>
5.1	Cell cultures .....	43
5.2	Cold Atmospheric Plasma irradiation .....	44
5.3	Viability assays .....	47
5.3.1	MTT .....	47
5.3.2	Sulforhodamine B .....	48
5.4	Statistical Analysis .....	49
5.5	Position Error of the Robot.....	51
<b>Chapter 6: Results and Discussion .....</b>		<b>53</b>
6.1	Accuracy of the Robotic System .....	53
6.2	Results and Discussion of the Application of CAP .....	56
6.2.1	Validation of the Robotic System .....	56
6.2.2	Biological Significance.....	70
6.2.2.1	ECC-1 .....	70
6.2.2.2	RL-95 .....	71
6.2.2.3	Hela .....	72
6.3	Evaluation of the Robotic System .....	73
<b>Chapter 7: Conclusion and Future Work .....</b>		<b>76</b>
<b>References.....</b>		<b>79</b>

# List of Figures

<b>Figure 1</b> – Human uterus scheme.....	5
<b>Figure 2</b> – Endometrial tumor, <b>a</b> : Grade 1; <b>b</b> : Grade 2; <b>c</b> : Grade 3 (adapted from [14]).....	7
<b>Figure 3</b> – Staging of endometrial cancer according to FIGO. ....	8
<b>Figure 4</b> – Scheme of the four states of matter and their interactions. ....	10
<b>Figure 5</b> – Skin regeneration with CAP treatment, <b>a</b> : before CAP treatment; <b>b</b> : after 7 treatment sessions of 2 minutes of irradiation; <b>c</b> : after 11 treatment sessions of 2 minutes of irradiation (adapted from [24]).....	11
<b>Figure 6</b> – Manual system of application of CAP within the laminar flow chamber. ....	14
<b>Figure 7</b> – Electrodes positioned for CAP discharge. ....	15
<b>Figure 8</b> – <b>a</b> : Scheme of a cartesian robot [42]; <b>b</b> : Scheme of a cylindrical robot [42]; <b>c</b> : Scheme of a robotic arm [42]; <b>d</b> : Robotic system of automatic pipetting [10]; <b>e</b> : Motoman dual arm robot operating [43]; <b>f</b> : Scheme of Veebot robot performance [44]; <b>g</b> : Scheme of the da Vinci robot performance [17]. ....	18
<b>Figure 9</b> – Identification of the diameter measured in the multiwell plates.....	20
<b>Figure 10</b> – Scheme of a well of a 48-well plate with diameter, radius and accuracy identified. ....	21
<b>Figure 11</b> – Laminar flow chamber.....	23
<b>Figure 12</b> – 3D draft of the linear actuators of the robot (adapted from [47]). ....	25
<b>Figure 13</b> – 3D draft of the piece for the support of the electrodes. <b>a</b> : oblique view; <b>b</b> : top view; <b>c</b> : front view. ....	28
<b>Figure 14</b> – 3D draft of the support to fix the well plates in the basis of the robotic system. <b>a</b> : top view with the dimensions in millimetres; <b>b</b> : oblique view; <b>c</b> : top view. ....	28
<b>Figure 15</b> – Robotic system developed. ....	30
<b>Figure 16</b> – Needle and syringe used as electrodes for CAP ejection. ....	31
<b>Figure 17</b> – Scheme of the robotic system performing CAP application.....	31
<b>Figure 18</b> – <b>a</b> : 24-well plate and <b>b</b> : 48-well plate for cell culture. ....	33
<b>Figure 19</b> – Identification of the wells of the multiwell plates, <b>a</b> : 48-well plate; <b>b</b> : 24-well plate.....	34
<b>Figure 20</b> – Scheme of an interaction. <b>a</b> : Selection of the well plate to irradiate (24 well-plate); <b>b</b> : Selection of the well to irradiate (well A1); <b>c</b> : “ok” button when the well is selected; <b>d</b> : Selection of the time to irradiate the well selected (15 seconds); <b>e</b> : If there is no more wells to irradiate, “Start” button is pressed; <b>f</b> : When “Start” button is pressed, a G-code file is returned.....	35
<b>Figure 21</b> – Pseudocode algorithm of the generation of the G-code file in the GUI. ....	36
<b>Figure 22</b> – Use Case scheme of the interaction between the user and the system. ....	40
<b>Figure 23</b> – Model of the process of manual CAP application. ....	41

<b>Figure 24</b> – Model of the process of CAP application with the robotic system. ....	42
<b>Figure 25</b> – Cell lines in culture, <b>a</b> : ECC-1 cells; <b>b</b> : Hela cells; <b>c</b> : RL-95 cells.....	44
<b>Figure 26</b> – Neubauer Chamber scheme (adapted from [56]).....	45
<b>Figure 27</b> – 48-well plate identified containing ECC-1 cells for CAP irradiation.....	47
<b>Figure 28</b> – Structure of MTT and Formazan [59]. ....	48
<b>Figure 29</b> – SRB structure and interaction (adapted from [61]).....	49
<b>Figure 30</b> – Scheme of the movements for the measurements.....	51
<b>Figure 31</b> – Boxplots of the results of the viability assays performed after ECC-1 CAP irradiation. <b>a</b> : SRB assay performed after manual irradiation; <b>b</b> : SRB assay performed after automatic irradiation; <b>c</b> : MTT assay performed after manual irradiation; <b>d</b> : MTT assay performed after automatic irradiation. The Bonferroni test is represented in the graphs and the statistical significance is represented by ▲ if $p < 0.05$ , ▲▲ if $p < 0.01$ and ▲▲▲ if $p < 0.001$ . ....	58
<b>Figure 32</b> – Boxplots of the results of the viability assays performed after RL-95 cell line CAP irradiation. <b>a</b> : SRB assay performed after manual irradiation; <b>b</b> : SRB assay performed after automatic irradiation; <b>c</b> : MTT assay performed after manual irradiation; <b>d</b> : MTT assay performed after automatic irradiation. The Bonferroni test is represented in the graphs and the statistical significance is represented by ▲ if $p < 0.05$ , ▲▲ if $p < 0.01$ and ▲▲▲ if $p < 0.001$ . ....	63
<b>Figure 33</b> – Boxplots of the results of the viability assays performed after Hela cell line CAP irradiation. <b>a</b> : SRB assay performed after manual irradiation; <b>b</b> : SRB assay performed after automatic irradiation; <b>c</b> : MTT assay performed after manual irradiation; <b>d</b> : MTT assay performed after automatic irradiation. The Bonferroni test is represented in the graphs and the statistical significance is represented by ▲ if $p < 0.05$ , ▲▲ if $p < 0.01$ and ▲▲▲ if $p < 0.001$ . ....	67

# List of Tables

<b>Table 1</b> – Grading classification of tumors [13]. .....	7
<b>Table 2</b> - Classification of the stage of endometrial carcinoma [7,16]. .....	8
<b>Table 3</b> - Comparison of some parameters of robotic mechanisms (adapted from [45-47]). .....	24
<b>Table 4</b> – Requirements for the design of the pieces to couple to the cartesian robot. ....	27
<b>Table 5</b> – Values of the measurements of the movements of the axes of the system. ....	55
<b>Table 6</b> - Coefficients of variation for manual and automatic technique of CAP application for ECC-1 cell line for SRB and MTT assay, n.s. (not significant).....	60
<b>Table 7</b> - Coefficients of variation for manual and automatic technique of CAP application for RL-95 cell line for SRB and MTT assay, n.s. (not significant). ....	65
<b>Table 8</b> - Coefficients of variation for manual and automatic technique of CAP application for Hela cell line for SRB and MTT assay, n.s. (not significant). ....	69



# List of Abbreviations

<b>ABS</b>	Acrylonitrile Butadiene Styrene
<b>ADM</b>	App Designer MATLAB
<b>AJCC</b>	American Joint Committee on Cancer
<b>ATP</b>	Adenosine Triphosphate
<b>BPMN</b>	Business Process Model and Notation
<b>CAD</b>	Computer Aided Design
<b>CAP</b>	Cold Atmospheric Plasma
<b>CNC</b>	Computer Numerical Control
<b>DMEM</b>	Dulbecco's Modified Eagle Medium
<b>DNA</b>	Deoxyribonucleic Acid
<b>DOF</b>	Degrees of Freedom
<b>FBS</b>	Fetal Bovine Serum
<b>FDM</b>	Fused Deposition Modelling
<b>FIGO</b>	International Federation of Gynaecology and Obstetrics
<b>FWHM</b>	Full Width at Half Maximum
<b>GUI</b>	Graphical User Interface
<b>HCL</b>	Hydrochloric Acid
<b>HNPCC</b>	Hereditary Nonpolyposis Colorectal Cancer
<b>iCBR</b>	Coimbra Institute for Clinical and Biomedical Research
<b>MTT</b>	3-(4,5-dimethylthiazol-2-yl)-2,5-diphenyltetrazolium bromide
<b>NC</b>	Numerical Control
<b>PBS</b>	Phosphate-buffered Saline
<b>PC</b>	Polycarbonate
<b>PET</b>	Polyethylene
<b>PFA</b>	Plasma Frio Atmosférico
<b>PLA</b>	Poly lactide
<b>ROS</b>	Reactive Oxygen Species
<b>RPMI</b>	Roswell Park Memorial Institute
<b>SRB</b>	Sulforhodamine B
<b>STL</b>	Standard Tessellation Language

<b>TAH-BSO</b>	Total Extrafascial Hysterectomy with Bilateral Salpingo-Oophorectomy
<b>TPE</b>	Thermoplastic Elastomers
<b>UI</b>	User Interface
<b>UV</b>	Ultraviolet



# Chapter 1: Introduction

---

Current automation technology allows the automatization of tasks that were previously performed by human labour, preventing time spending in less value-added tasks and increasing human workers wellbeing at work. Automation technologies are fundamental to keep up with the constant evolution of companies and the global economy. Robotics, human-machine interfaces and artificial intelligence have been gaining interest in many areas, from industry to services to health.

Humans and machines working together for the improvement of medicine and healthcare is one of the main goals in medical robotics research. Technology has already provided robotic solutions capable of performing some human supportive tasks for health professionals, such as surgeries, physiotherapy and occupational therapy. In medical and biology research, automatization of laboratory techniques is emerging constantly with new solutions being developed, namely in automatic manipulation [1].

The automatization of tasks is important in the medical investigation field in order to make researchers' work time more productive. Repetitive tasks are often required in medical investigation laboratories which translates in the need for robotic solutions that can autonomously perform human tasks with precision.

In the Biophysics Institute of the University of Coimbra, Portugal, the exposure of cell cultures to CAP is currently being performed to study its potential in cancer treatment. The procedure of exposing cell cultures to CAP, however, is currently a fully manual laboratory technique, performed completely by hand. Thus, being a repetitive and systematic routine, it becomes exhausting and time-consuming for the researcher, therefore prone to human error and with low reproducibility.

Worldwide, endometrial cancer rate incidence in women is one of the highest of the gynaecological cancer types [2]. Currently, the diagnosis is made, often, in early stages of the disease and the treatment is primarily surgical. However, given that the currently available treatment approaches do not guarantee cancer cure, there is the need to develop new strategies that can enhance the response, particularly for increasing incidence cancers – namely, the endometrial cancer [3].

## 1.1 PROBLEM AND MOTIVATION

Currently, in the Biophysics Institute of the University of Coimbra, the irradiation of cell cultures with CAP is made in multiwell plates, through a handmade and repetitive task that demands high time investment.

In a simplified manner, the exposure of cell lines to CAP consists of manually positioning two electrodes in specific positions on each well of the multiwell plates containing the cell cultures and the cell culture media, in order to produce an electric field that is responsible for the discharge of plasma into the cells. Besides being time-consuming, this manual operation can negatively influence the results of research studies, because it is a source of random errors in the electrode positioning and a source of cultures' contamination, due to high human manipulation.

The present study emerged to answer these difficulties identified in the Biophysics Institute of the University of Coimbra. Therefore, this project aimed to automatize the cell cultures' exposure to CAP, increasing the rentability of researchers' working time and improving the reproducibility of the procedures.

## 1.2 PROPOSED APPROACH

This project aimed to implement a solution to the aforementioned problem, by constructing a robotic system capable of automatizing the exposure of cell cultures to CAP, simplifying the procedure, decreasing the time spent with it, avoiding human errors, and improving the reproducibility of the assays.

A detailed study about the technique of cell cultures' exposure to CAP was carried out, in order to identify all the requirements and necessities of the system to be implemented. The robotic system was adapted, programmed and tested. As a proof of concept, *in vitro* studies were performed to evaluate the cytotoxicity of CAP in tumor cells, using three cell lines of endometrial cancer. To validate the developed approach and study the system reproducibility, the tests were performed both with the previous manual system of CAP discharge and with the newly developed robotic system.

### 1.3 THESIS OVERVIEW

The present thesis is divided into seven chapters that aim to describe the development of the work that lead to this dissertation, from the study of the state of the art and contextualization to the experimental work and conclusions of the project.

The **first two chapters** present the contextualization of the problem and the literature review, with an introduction to the main topics related to the study, namely robotics, cold atmospheric plasma and endometrial cancer.

The **third chapter** describes the planning and development of the constituents of the robotic system constructed within the present project. Then, the **fourth chapter** details about the developed Graphical User Interface (GUI) to allow the users' interaction with the robotic system in an easy and intuitive manner. The **fifth chapter** describes the protocols and procedures performed to validate the robotic system for the exposure of the endometrial tumor cells to CAP.

Lastly, **chapter 6** presents the analysis and discussion of the validation tests of the robotic system. **Chapter 7** concludes the dissertation and proposes suggestions for future work.



# Chapter 2: Literature Review

---

## 2.1 ENDOMETRIAL CANCER

The endometrium is the inner tissue layer of the uterus (**Figure 1**), where the implantation of the embryo takes place. During reproductive years, endometrium suffers a complex succession of changes as a result of the menstrual cycle, with a typical duration of 28 days [4]. During these cycles, the proliferative activity of endometrium underlies continuous cell division, a process prone to errors that can ultimately promote tumorigenesis.

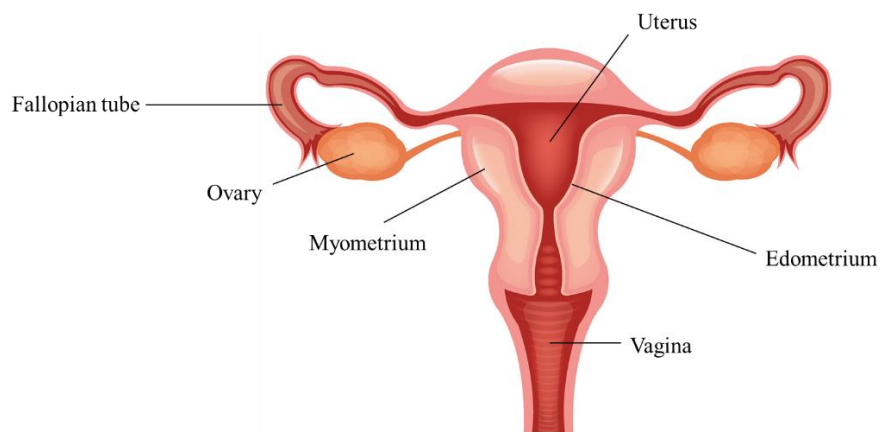


**Figure 1** – Human uterus scheme.

A tumor is an abnormal mass of tissue resultant of uncontrolled cell growth and can be classified as benign or malignant. Malign tumors, also called neoplasms, or collectively referred as cancers, can be fatal since they can invade and destroy adjacent and distant tissues or organs [5].

In developed countries, endometrial cancer has been emerging as the most common gynaecological cancer in women, representing 6% of cancers in women, and its incidence rate is expected to keep rising. The incidence rate is typically higher in developed countries including the United States of America and Occidental Europe, and lower in Africa, Asia and Latin America [6-8].

Despite the elevated incidence, the mortality rate is low because of the early diagnosis in developed countries. The prognosis of endometrial carcinoma is determined by disease stage and histology. However, most of the patients are diagnosed in early stages of the disease and with favourable histologic type. Therefore, most women have a good prognosis [9].

Endometrial cancer is considered a neoplasm with epithelial origin, so, it must be staged as a carcinoma. From a biological point of view, endometrial carcinoma is divided in 2 types: I and II [6-7].

Type I is the most frequent one and it is responsible for about 80-90% of the cases. It occurs more frequently in young women, usually obese and with a background of estrogen stimulation. This type of tumor is associated with endometrial hyperplasia and well-differentiated; it superficially invades the myometrium and has a better diagnosis.

Type II is less frequent, representing 10-20% of the cases. It is independent of estrogen stimulation and its incidence is higher in older, post-menopause and thin women. Type II tumors are often large bulky tumors or deeply invasive into the myometrium and are often spread outside of the uterus at the time of diagnosis, so, usually, its prognosis is not favourable [10-11].

There are also some risk factors identified such as nulliparity, late menopause, the use of oral contraceptives, heredity, tamoxifen, obesity, early menarche and estrogen exposure [12].

Publicized studies have defined a classification system for grading endometrial tumors based on the solid tumor growth, as shown in **Table 1** and **Figure 2** [12].

Generically, type I carcinomas present glandular growth patterns and can be classified in 3 histologic grades: almost entirely composed of well-formed glands, well differentiated tumor (Grade 1); well-formed glands mixed with areas of aggregates of cells, moderately differentiated tumor (Grade 2); and above 50% of differentiated solid growth, poorly differentiated tumor (Grade 3).

On the other hand, type II carcinomas are characterized as being poorly differentiated Grade 3 tumors [11].

**Table 1** – Grading classification of tumors [13].

<b>GX</b>	<b>The grade cannot be evaluated</b>
<b>Grade 1</b>	Under 5% of differentiated solid growth Tumor cells well differentiated ( <b>Figure 2-a</b> )
<b>Grade 2</b>	Between 5 and 50% of differentiated solid growth Tumor cells moderately differentiated ( <b>Figure 2-b</b> )
<b>Grade 3</b>	Above 50% of differentiated solid growth Tumor cells poorly differentiated ( <b>Figure 2-c</b> )

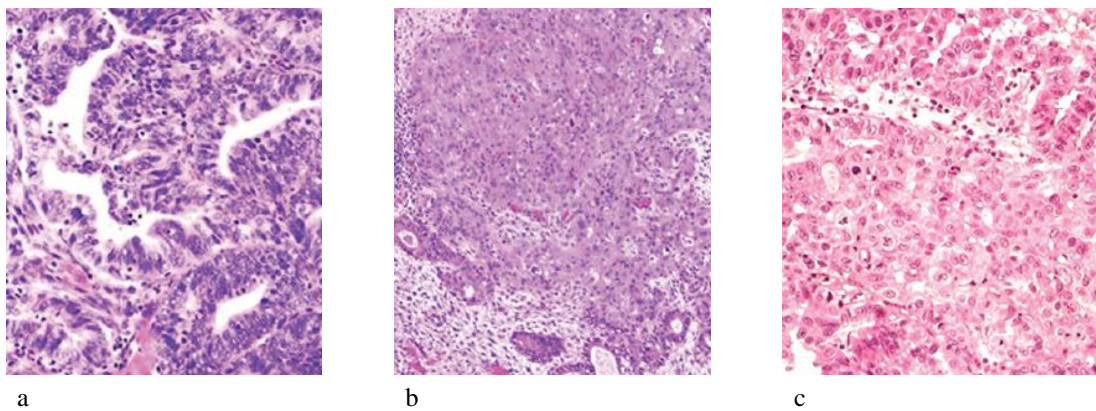


**Figure 2** – Endometrial tumor, **a**: Grade 1; **b**: Grade 2; **c**: Grade 3 (adapted from [14]).

Endometrial carcinoma is surgically staged according to the joint International Federation of Gynecology and Obstetrics (FIGO) and the American Joint Committee on Cancer (AJCC) TNM staging system. Staging allows to plan the best type of treatment. When the tumor is limited to the uterus, it is labelled as in Stage I. If the tumor has spread from the uterus to the cervical stroma, it is classified as in Stage II. When the tumor spreads to other local tissues of the pelvic area, it is in Stage III. Lastly, when the tumor presents metastasis in other parts of the body, Stage IV is considered (see **Table 2** and **Figure 3**) [15]. According to the TNM staging system, the tumor is classified based on its size and extent (T), spread to regional lymph nodes (N), and the involvement of metastases (M) [10].

**Table 2** - Classification of the stage of endometrial carcinoma [7,16].

	FIGO	TNM	
Stage I	IA	T1a N0 M0	Tumor limited to the endometrium
	IB	T1b N0 M0	Incursion of intern part of miometrium
	IC	T1c N0 M0	Incursion of external part of miometrium
Stage II	IIA	T2a N0 M0	Spread to endocervical mucosa
	IIB	T2b N0 M0	Incursion of the stroma of the cervix
Stage III	IIIA	T3a N0 M0	Incursion of uterine serosa and/or ovaries and fallopian tubes
	IIIB	T3b N0 M0	Vaginal metastasis
	IIIC	T3c N1 M0	Metastasis in pelvic nodes
Stage IV	IVA	T4 N0/N1 M0	Incursion of the mucosa of the bladder/rectum
	IVB	T4 N0/N1 M1	Distance metastasis and/or spread to lymph nodes in the groin area

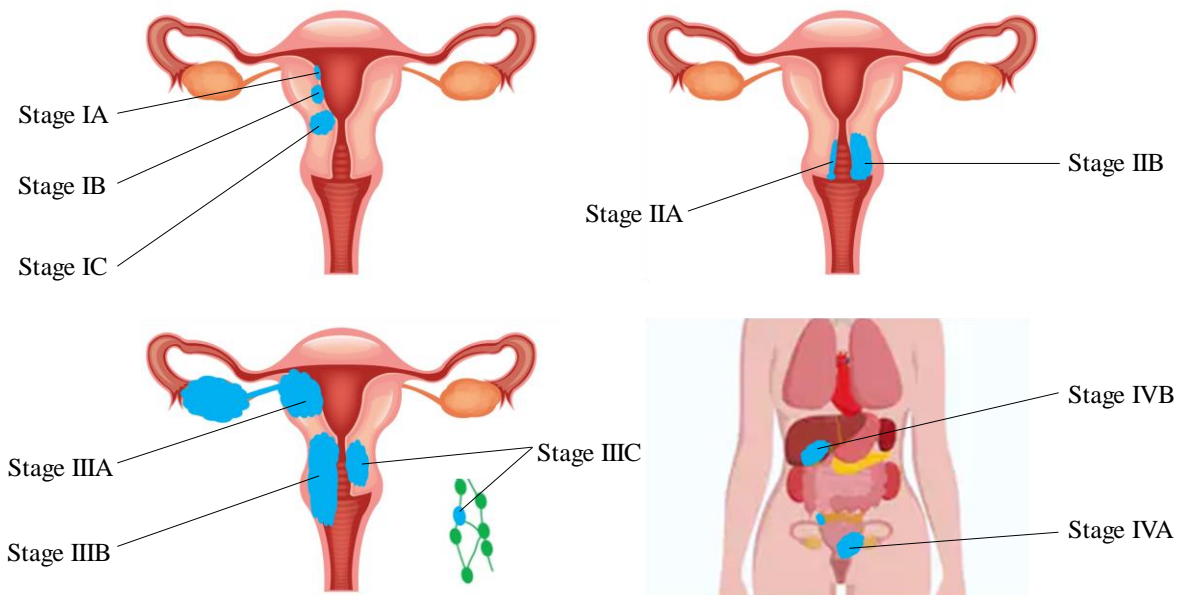


**Figure 3** – Staging of endometrial cancer according to FIGO.



### **2.1.1 THERAPIES IN ENDOMETRIAL CANCER TREATMENTS**

Routine screening of asymptomatic women at average or increased risk of endometrial carcinoma is not advised. There are no high-quality data to support the efficacy of screening for reducing endometrial cancer mortality.

Hereditary tumors represent 5% of the cases of endometrial cancer, and half of these correspond to situations of women with hereditary nonpolyposis colorectal cancer (HNPCC), also known as Lynch II syndrome. These women may constitute an exception since they constitute a group of risk of endometrial cancer, so, medical counselling must be considered in these cases [6].

Currently, endometrial cancer is initially managed with total extrafascial hysterectomy with bilateral salpingo-oophorectomy (TAH-BSO) performed either via laparotomy or laparoscopy, which consists in the removal of the uterus. Nevertheless, women presenting a tumor in stage IA, grade 1, can opt to avoid the surgery and, in that case, the alternative is hormone therapy (progestin therapy) [17].

Radiotherapy is mainly used as an adjuvant therapy in TAH-BSO in endometrial cancer treatment. It can be performed by vaginal brachytherapy, a type of intern radiotherapy, in which a radioactive material is inserted inside or next to the region to be treated, or it can be performed by external radiotherapy, where the radioactive source is outside of the body [6,18].

Publicized studies have demonstrated that brachytherapy allows a good vaginal control and presents a favourable toxicity when compared to external radiotherapy. Besides, radiotherapy efficiency in stages I and II demonstrates a reduction in recurrence, but no impact in the survival rate. Radiotherapy can be applied as soon as the surgical cicatrisation process is completed, until 12 weeks after the surgery, except for the cases when adjuvant chemotherapy is necessary [6,18].

Chemotherapy uses drugs to kill tumor cells and it is commonly used as an adjuvant therapy, when the tumor has spread to other parts of the body beyond the endometrium. For tumor in stages IB, grade 3 and in stage II, chemotherapy as an adjuvant therapy is under investigation. For tumors in stage III and for patients that

present metastases, published results have demonstrated that chemotherapy treatment is advisable [6].

## 2.2 COLD ATMOSPHERIC PLASMA

### 2.2.1 CHARACTERISTICS OF COLD ATMOSPHERIC PLASMA

Followed by solid, liquid and gas, plasma emerges as the fourth state of matter and has unique properties, **Figure 4**.

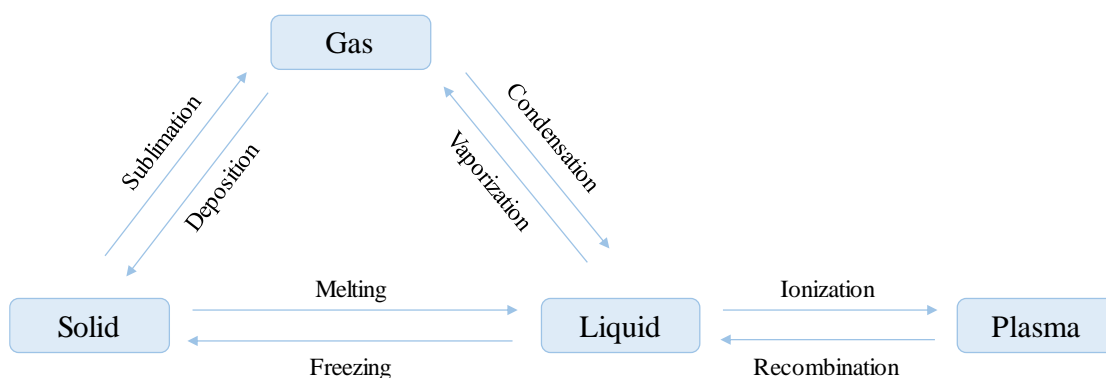


**Figure 4** – Scheme of the four states of matter and their interactions.

In the field of medicine, plasma is a relatively new discover and it has been gaining interest and promoting interdisciplinarity by combining the fields of physics, biology and chemistry [19].

Plasma can be obtained by heating or ionizing a gas and its classifications can be based on density or temperature since there are various types of plasmas. CAP is a non-thermal plasma and its temperature is, approximately, room temperature. CAP is formed by a mixture of positive and negative ions and electrons, it emits ultraviolet (UV) radiation and can origin reactive species. Reactive species may induce both cell death and cell proliferation, depending on their concentration. When in large

concentrations, reactive species may induce Deoxyribonucleic Acid (DNA) damage in cells, which results in apoptosis and other forms of cell death [19].

### 2.2.2 APPLICATION OF PLASMA IN MEDICINE

Plasma has been used for several biomedical applications, such as skin regeneration, cancer therapy, blood coagulation, cosmetics and sterilization. Published studies have shown that plasma, depending on its specific conditions can have different properties [20].

For damaged tissues, plasma appears to demonstrate a capability to potentiate cell proliferation and consequently accelerate skin regeneration [21]; also, plasma promotes a fast blood coagulation to support healing of damaged tissues [22]. In **Figure 5** is portrayed a clinical practice of CAP treatment for skin regeneration.

CAP has been used to foster the regeneration process since, when applied in cells at specific conditions, it is capable of inducing cell division and increasing the content of Adenosine Triphosphate (ATP), hence, accelerating the tissue regeneration process [23].



**Figure 5** – Skin regeneration with CAP treatment, **a**: before CAP treatment; **b**: after 7 treatment sessions of 2 minutes of irradiation; **c**: after 11 treatment sessions of 2 minutes of irradiation (adapted from [24]).

Decontamination of superficies and tissue sterilization is another application of CAP. Studies have been demonstrating the efficiency of CAP in fungi and bacteria removal for sterilization [25-26]. When it is applied in this context, CAP damages

DNA, and while these lesions are easily outbalanced by eukaryotic cells, they are not overcome by bacteria and fungi. This particularity makes CAP useful for applications such as sterilization, due to its selectivity to eliminate bacteria and fungi [23].

Studies have also shown that CAP has potential properties in electrosurgery, a surgery where tissue is removed with high precision without interfering with adjacent tissues. CAP has the potential to induce the detachment of the cells from the tissue. In the field of cosmetics, CAP is emerging as a new approach for Hailey-Hailey disease (skin disease) therapy due to the potential for skin regeneration [22,25].

It is suggested that the different effects of CAP in cells are based on the electric field associated to CAP. Lower electric fields stimulate cell division, whereas, on the other hand, higher electric fields are responsible for cell death. Studies concerning CAP and its applications are currently very limited. Despite the largely unknown mechanisms, CAP can eliminate bacteria and fungi without causing any pathology on cells [23].

In the field of oncology, CAP is gaining interest because it has been demonstrated that, when in contact with living cancer cells, it has the capacity of inducing cell apoptosis. It also demonstrates selectivity only to cancer cells without damaging surrounding tissue [23].

### **2.2.3 COLD ATMOSPHERIC PLASMA IN CANCER TREATMENT**

In medicine, CAP is emerging as a revolutionary basis for the treatment of tumors. CAP mechanisms of action are still little known, however, there are some hypotheses suggested.

Direct effect of UV radiation in cells may induce apoptosis. When UV radiation, produced by plasma, is absorbed by cells, it can induce direct effects in DNA and cause disturbances in RedOx cell balance, leading to cell death [27].

Another hypothesis is that CAP can have in its complex constitution some toxic components (  $H_2O_2$  and NO) that, when in contact with cells, may induce cell death. Reactive species derived from oxygen and nitrogen can induce morphologic changes,

DNA damage, membrane depolarization and cause cell death [25]. In other words, significant variation of intracellular levels of reactive oxygen species (ROS) and nitrogen can result in the increase of RedOx reactions, and consequently, induction of cell death by DNA damage.

Electric fields can induce apoptosis and represent another proposed mechanism of action of CAP [19]. Electric fields can act via changing the membrane permeability, cell growth, DNA structure and synthesis, mitosis and interfere with increased calcium permeability [25].

Despite all these hypotheses, there is no consensus yet concerning the exact mechanism of CAP performance [28].

Another recent suggestion about the CAP mechanism is the action of a reactive molecule, ozone ( $O_3$ ), present in the complex plasma constitution. Studies suggest that  $O_3$  induces cell death and, as the CAP exposure time increases,  $O_3$  concentration increases as well and, consequently, cell death increases [29].

#### **2.2.4 SYSTEM OF APPLICATION OF COLD ATMOSPHERIC PLASMA**

Several devices for production and application of CAP in cell lines have been developed in the last years. These devices vary in size, shape and design depending on their specific function. There is no standard model, so, in each specific case, the requirements and conditions must be studied.

Generically, CAP devices can be classified as direct, indirect or hybrid plasma sources according to the electrode configuration characteristics and the way of use for the treatment.

In direct plasma sources, the target tissue/area is used as a counter electrode and integrates the electric circuit. This allows the direct contact between produced plasma and the target area.

Indirect plasma sources make use of two electrodes to generate the plasma and posterior transportation to the target area through a gas flow. These devices can vary in size, configuration and jets.

Hybrid plasma sources combine the plasma production technique of direct sources and the property of indirect sources since the created current does not cross the target area [25,30,31].

At the Biophysics Institute, CAP is produced in an indirect source, a device developed in-house, whose properties and characteristics will not be presented due to intellectual property reasons. CAP is produced in this device and, for the application in cells, it is conducted in electrodes.

Until the beginning of this study, the solution used for the application of CAP in the compartments of multiwell plates was constituted by two universal supports to fix the electrodes that conduct the plasma to the cells, as depicted in **Figure 6**. The needles are connected by electric plugs to the CAP producing device, and work as electrodes to conduct CAP flux.

It is important to notice that, in the present study, only the CAP application system was renewed. The CAP production device is outside of the aim of the project.

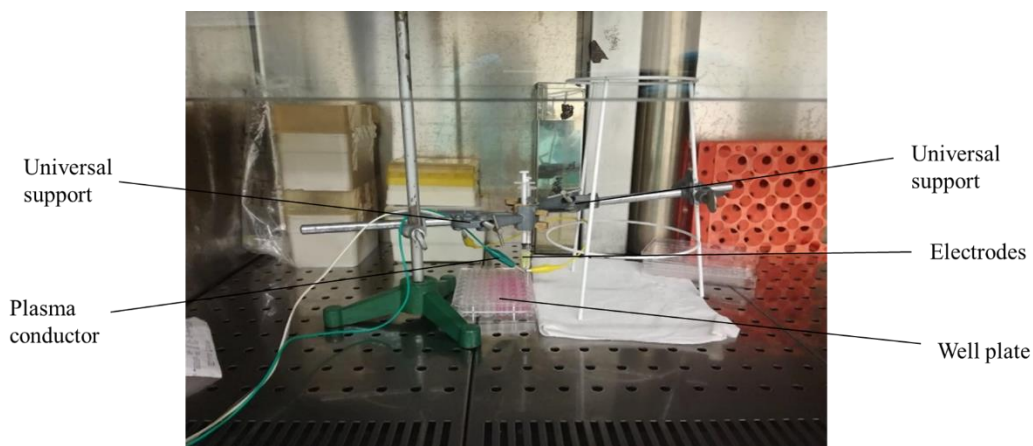


**Figure 6** – Manual system of application of CAP within the laminar flow chamber.

Once the electrodes are fixed in the support, there is the requirement for the user to manually positioning the two electrodes inside the well of the multiwell plate containing the cells to irradiate with CAP, as in **Figure 7**. For the manual CAP application, it is used a conventional support system where the multiwell plate and the electrodes are moved manually and, in this way, there is no complete control of the local of the well where the plasma discharge occurs.

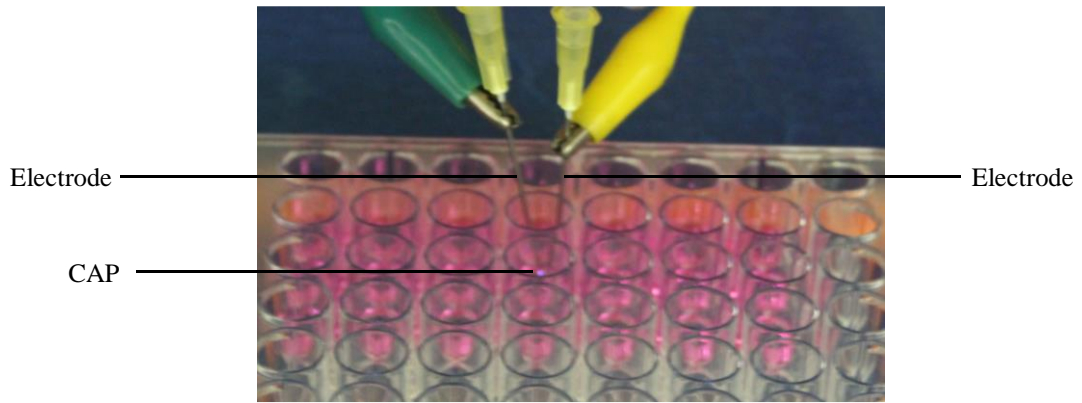


**Figure 7** – Electrodes positioned for CAP discharge.

This technique often causes contaminations of the cells, due to the constant contact of the user with the electrodes very close to the plate. Also, since the discharge of CAP is position dependent, this technique, performed manually, demands a lot of time and concentration from the researcher. The reproducibility of the technique is a very important factor that can be compromised since the task, manually performed, is prone to errors associated with the human operation.

### **2.3 ROBOTIC-BASED SOLUTIONS**

The rapid expansion of robotics has aroused interest in different domains, including the medical domain.

It is believed that the concept of using robots to support and execute several human tasks has been in humans' mind over thousands of years. Nevertheless, in medicine and medical research, robots only began to emerge 30 years ago [32-33].

In recent years, the development of increasingly complex robots has been gaining interest in multiple automation applications [34]. Scientific and technological communities have been following the exponential growth of robotics and its solutions have been studied to interpret human tasks as effectively as possible.

Collaborative robots have appeared to respond and support human tasks in a synergetic way [34]. Three to four decades ago, the robotic systems were mainly developed to carry out repetitive tasks with minimal interaction with the surroundings,

making difficult its application in the medical field. Therefore, there was an evolution into more safe and cooperative systems and Human-Robot interaction in order to introduce robots into medical laboratory environments [32].

A very wide range of medical laboratory research experiments require rigorous measurements and handling of solutions in specific positions. In medicine, robotic systems have been emerging both to perform repetitive tasks (such as pipetting) and to be used as diagnostic tools. These repetitive tasks are highly time-consuming processes that often translate into the decrease of time rentability of researchers in the laboratory.

Collaborative robots must have a set of strict requisites in order to work safely in collaboration with humans in the same workspace. It is essential that the response to obstacles is extremely fast and precise.

### **2.3.1 ROBOTS IN BIOMEDICAL RESEARCH**

In recent years, the market of collaborative robots for medical laboratories have been growing in an exponential way. From the simplest to the most complex robots, automation of human tasks and techniques, such as object manipulation (test tubes, pipettes, well plates, etc), is emerging as a revolutionary new way of medical laboratory investigation.

It will be presented some types of robotic solutions available to support humans in the execution of laboratory and medical tasks.

Cartesian robots are characterized by having three degrees of freedom (DOF) robots and one of the most simple type of robots [35-36]. These robots possess a geometry analogous to a XYZ coordinate system, as shown in **Figure 8-a**. This geometry can simply be applied to collaborative work in laboratories for simple repetitive tasks such as pipetting [37].

The cylindrical robot is a type of robot with four DOF, similar to the cartesian robot but with a rotation axis, as the example of **Figure 8-b**. It is mainly used to support chromatography techniques such as sample extraction and injection [37].



Articulated robots are another of the simplest types of robots. This robot is more versatile for laboratory techniques applications than the two presented above, since it has more DOF. It works as a robotic arm and has shoulder, elbow and wrist joints, which makes the robot very adaptable to many types of movements, as represented in **Figure 8-c** [37].

Pipetting is one of the most repetitive and time-consuming tasks in biomedical research laboratories. The pipetting robot presented here is the result of the work of a colleague from the University of OPorto, Portugal, and consists of a system constituted by a robotic arm coupled to a gripper for the pipette [32]. This robotic system is able of automatize the entire process of pipetting a liquid solution to the wells of well plates, as the example shown in **Figure 8-d**.

Yaskawa developed a robot designed with the ability to accomplish biomedical laboratory tasks such as pick and place petri dishes, opening eppendorfs, put and take covers of containers and manage pipettes. The dual arm robot is constituted by two robotic arms with seven DOF each, as shown in **Figure 8-e**. This robot is capable of increasing the speed of the tasks allied to a higher precision and avoid the direct contact between the researcher and potentially toxic and dangerous substances [38].

Veebot, represented in **Figure 8-f**, is a robot used to perform needle insertion, taking advantage of medical imaging, computer vision and machine learning to identify and track the target, verify and align the target insertion site, and insert the needle. The robot combines infrared light source and ultrasound to detect and select a suitable vein and inserts the needle with 83% of accuracy [39-40].

The da Vinci robot, shown in **Figure 8-g**, is the most iconic robot in medicine, since it can execute high precision and sensible non-invasive surgeries. Surgeons can also control the robot at long distances. It consists of four robotic arms connected to a manipulator and a console that allows the surgeon to control the movements of the robotic arms with a high degree of precision [41].

Undeniably, there are already many devices and collaborative robots available to support humans in many different types of tasks and procedures in medical laboratory research. However, they are normally relatively expensive and difficult to operate for non-experts in robotics. In the present study, the main goal is to engineer a low-cost user-friendly automatized system for the application of CAP in cell lines.

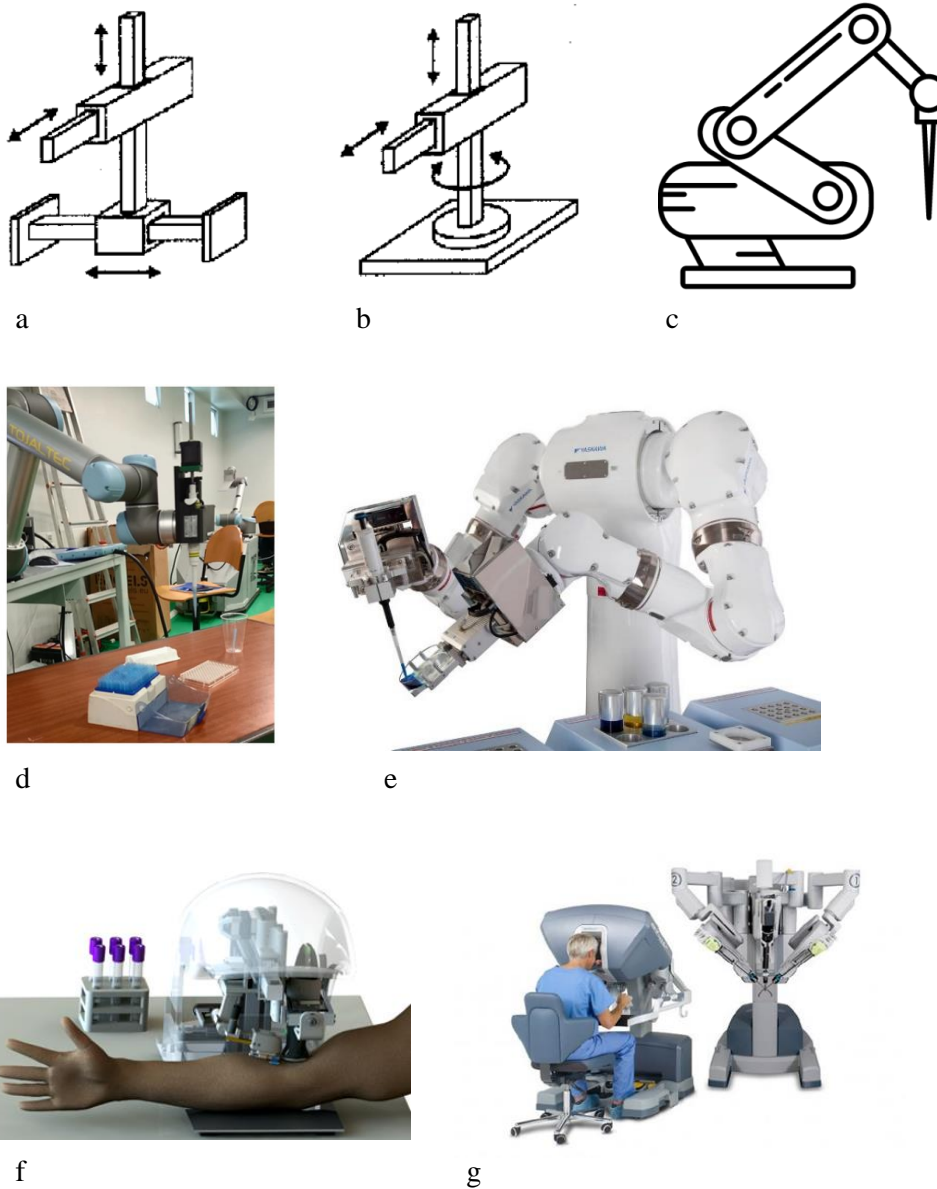


**Figure 8** – **a**: Scheme of a cartesian robot [42]; **b**: Scheme of a cylindrical robot [42]; **c**: Scheme of a robotic arm [42]; **d**: Robotic system of automatic pipetting [10]; **e**: Motoman dual arm robot operating [43]; **f**: Scheme of Veebot robot performance [44]; **g**: Scheme of the da Vinci robot performance [17].

# Chapter 3: Robotic System

---

In this chapter, all the components used for the development of the robotic system are described.

## 3.1 REQUIREMENTS

In the first stage of the development of the automated system, there was the identification of relevant requirements needed to implement a robotic solution capable of substituting the manual system described in **chapter 2**, section 2.2.4, and performing CAP irradiation in cell lines in an autonomous way, in the laboratory of the Biophysics Institute.

To develop the robotic system, all the relevant requirements for its performance in the laboratory had to be rigorously identified. The requirements can be sub-divided in functional and non-functional requirements. Functional requirements are directly related to the performance of the system, namely what is the robotic system purpose and identifying the criteria to operate. Non-functional requirements are related to the work and environment conditions of the robotic system.

### 3.1.1 FUNCTIONAL REQUIREMENTS

The accuracy of the robot is a fundamental criterion for the application of CAP since the electrodes need to be at specific positions and the application is performed in well plates. In this context, to establish the robot accuracy, we considered the diameter of the wells, in 24 and 48-well plates.

It was considered that the minimum accuracy needed for the system should be, approximately, half of the radius of the smaller measured diameter. This limit was established because that is the minimum error that we can use to ensure that the position of the electrodes is positioned inside the wells. Following are presented the

calculi of the average diameter measured from the 24 and 48-well plates (**Figure 9**), using **Equation 1**, and its standard deviation, in **Equation 2**.

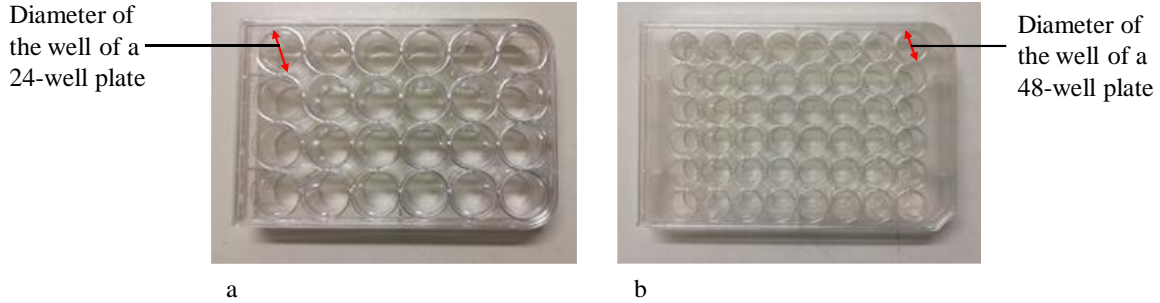


**Figure 9** – Identification of the diameter measured in the multiwell plates.

$$\text{Mean} = \bar{x} = \frac{\sum x}{n} \quad (1)$$

$$\text{Standard deviation} = s = \sqrt{\frac{\sum(x_i - \bar{x})}{n - 1}} \quad (2)$$

Where  $\bar{x}$  = mean,  $n$  = number of observed values,  $s$  = standard deviation and  $x_i$  = observed values.

$$\text{Mean}_{24\text{-well plate diameter}} = \bar{x} = \frac{\sum x}{24} = 15.62 \pm 0.01 \text{ mm}$$

With 0.01 being the uncertainty associated with the digital caliper used to measure the diameter.

$$\text{Standard deviation}_{24\text{-well plate diameter}} = s = \sqrt{\frac{\sum(x_i - \bar{x})}{n - 1}} = 0.04 \text{ mm}$$

$$\text{Mean}_{48\text{-well plate diameter}} = \bar{x} = \frac{\sum x}{48} = 11.01 \pm 0.01 \text{ mm}$$

$$\text{Standard deviation}_{48\text{-well plate diameter}} = s = \sqrt{\frac{\sum(x_i - \bar{x})}{n - 1}} = 0.02 \text{ mm}$$

Taking into consideration the obtained results, to calculate the accuracy needed, it was considered the minimum diameter calculated, which corresponds to the diameter of the 48-well plate,  $11.01 \pm 0.01 \text{ mm}$ , so, to calculate the minimum accuracy, it was established that the minimum limit is half of the radius of the well (see **Figure 10**).

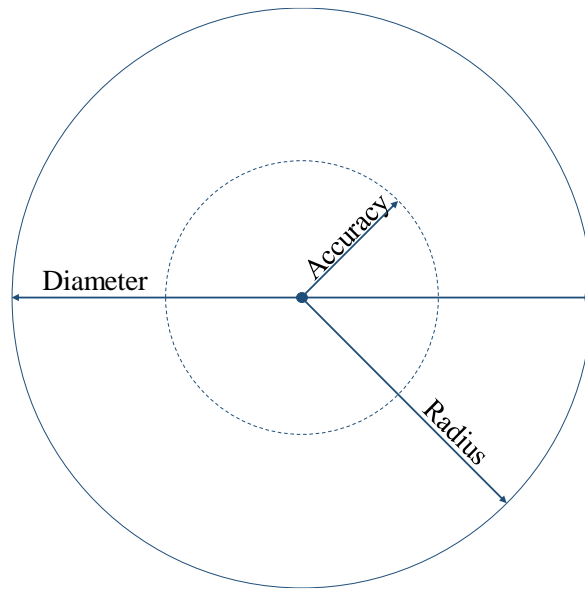


**Figure 10** – Scheme of a well of a 48-well plate with diameter, radius and accuracy identified.

$$\text{Radius}_{48\text{-well plate diameter}} = \frac{\text{Mean}_{48\text{-well plate diameter}}}{2} = 5.51 \pm 0.01 \text{ mm}$$

$$\text{Accuracy} = \frac{\text{Radius}_{48\text{-well plate diameter}}}{2} = 2.75 \pm 0.01 \text{ mm}$$

With the calculi presented above, it could be concluded that the minimum accuracy needed for the robotic system is  $2.75 \text{ mm}$ .

Another requirement identified is the number of DOF. The purpose of the system is to perform the application of CAP in well plates, and for that, the system must have the ability to move in longitudinal, horizontal and vertical axis, moving from one well

to another in the simplest trajectory. So, the minimum number of DOF for the system is three.

The robotic system must also have a specific area to couple the electrodes, responsible for CAP conduction, an end-effector. The end-effector enable the user to easily change the syringe and needles, that work as the electrodes, and adjust their position for CAP discharge.

Additionally, the development of a GUI is important for the system. Human-Machine interaction requires the development of a user-friendly interface in order to facilitate the control and programming of the robotic system for the customization of the CAP irradiation in each application. Hence, it is required the development of an interactive interface adapted to the robotic system.

### 3.1.2 NON-FUNCTIONAL REQUIREMENTS

To identify the non-functional requirements, an evaluation of the workspace of the system was performed, in order to analyse any possible physical limitation.

The system's workspace is inside the laminar flow chamber of the laboratory, since it is to work with cell cultures and sterilized material. In such scenario, the robotic system must fit within the area of the laminar flow chamber placed in the laboratory of the Biophysics Institute. The dimensions of this laminar flow chamber were measured and registered, presenting the values of  $119.00 \pm 0.01$  cm of width,  $50.01 \pm 0.01$  cm of length and  $65.50 \pm 0.01$  cm of height (**Figure 11**).



**Figure 11** – Laminar flow chamber.




Furthermore, the system must be able to irradiate well plates, so, the working area of the robotic system must be slightly bigger than the dimensions of a well plate to assure that the robotic system will be able to reach every well of the multiwell plates, which are  $85.48 \pm 0.01$  mm of width and  $127.76 \pm 0.01$  mm of length.

Considering these essential requirements for the development of the robotic system, it was established that the best solution for the system was a cartesian robot, since it is a low-cost solution that fits the conditions needed.

### **3.2 ROBOTIC MECHANISM**

For the development of the robotic mechanism, it was conducted an analysis on the solutions available in terms of linear actuators considering the requirements specified in section 3.1. A research on cartesian linear robots, composed by 3 linear actuators, was performed and the solutions that fitted in the specified parameters were saved to be compared to choose the most adequate. The final three robotic mechanisms selected are presented in **Table 3**.

**Table 3-** Comparison of some parameters of robotic mechanisms (adapted from [45-47]).

Robot mechanism	Picture	Accuracy	Dimensions	DOF
1		0.05 mm	50x50x50 cm	3
2		X and Y axis: 0.012 mm Z axis: 0.004mm	50x40x45 cm	3
4		0.05 mm	50x50x50 cm	3

The dimensions of all the mechanisms are suitable for the requirements, as they all fit inside the laminar flow chamber. The accuracy is also suitable in all the presented mechanisms, since it is smaller than the established limit: 2.75 mm. The number of DOF is three for all the mechanisms presented in **Table 3**, so they are equal concerning this parameter.

Comparing the values of accuracy, the lower value corresponds to mechanism number 2, which represents an advantage, making this the option to use.



Furthermore, for the selection of the linear actuators of the robot, it was considered that there were adaptations to be made in this system.

The development of pieces to adapt the system for coupling the electrodes (an end-effector) responsible for CAP discharge was required, as well as a solution to fix the multiwell plates in the basis, to avoid errors in the positioning. In **Figure 12**, it is possible to see that the cartesian robot number 2 has an area to couple an end-effector and the basis is a table, which facilitates the support of the well plates. Therefore, for the development of the present study, the mechanism considered as the best option was the number 2. **Figure 12** shows a 3D model of the system.

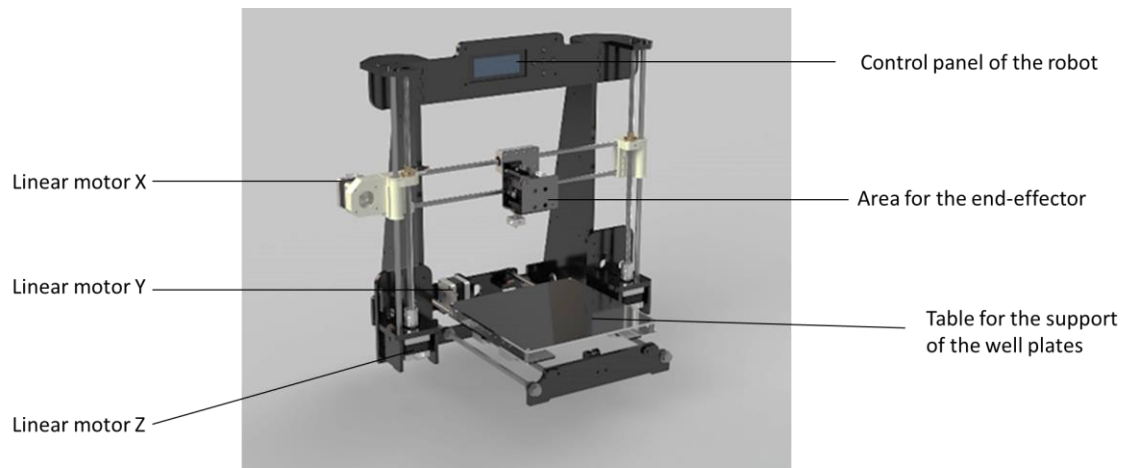


**Figure 12** – 3D draft of the linear actuators of the robot (adapted from [47]).

The cartesian robot was then manually assembled and calibrated in the Department of Mechanical Engineering of the University of Coimbra. The robot is constituted by three linear motors, each one working in perpendicular axes, X, Y and Z. The dimensions of the table of the cartesian robot, which is the work area of the cartesian robot identified in **Figure 12**, are 220 mm width per 220 mm length. The dimensions of the multiwell plates are 85.48 mm width per 127.76 mm length, as already mentioned, so, the system for CAP application must cover this area. Since the dimensions of the robot's working area are broader, this robot has the capability to cover the entire well plate, which means that its dimensions are adequate to meet the requirements.

### 3.3 END-EFFECTOR

This sub-chapter describes the development of an end-effector to assembly to the cartesian robot with the finality to support the electrodes in a fixed position for the irradiation of CAP. A support to fix the well plate was also developed.

The purpose of the end-effector is to be easily adjustable for adapting the position of the electrodes. In the robotic system, only the electrodes are directly exposed to cell cultures, and since the system can be applied in many types of cells, the electrodes must be disposable and sterilisable, which requires an easy system of changing the electrodes (needles). The end-effector and the support for the well plate were designed and posteriorly made by the technique of Fused Deposition Modelling (FDM) additive manufacturing using a 3D printer machine. This technique is easy to use and allows to obtain complex pieces with low cost material and equipment in short time [48]. FDM by 3D printing consists of deposition of layers on top of each other to build the pieces using a 3D printer machine.

The end-effector and the support were projected in a computer-aided design (CAD) software, the Autodesk Inventor. With the increasing development of technology, CAD drafting has been emerging as an advantageous tool for industry to design and model products [49]. In the present study, CAD was used to design and project:

- an end-effector to couple to the robot and serve as a support for the electrodes of the system of application of CAP;
- a support to fix the plates in the basis of the system.

The CAD software also allowed a virtual simulation of the behaviour of the pieces and their production by additive manufacturing.

Each CAD part was individually designed and later assembled in order to enable specific and detailed modifications in them, before their production.

Both the support of the electrodes and the support of the well plates were designed following the requirements listed in **Table 4**.

**Table 4** – Requirements for the design of the pieces to couple to the cartesian robot.

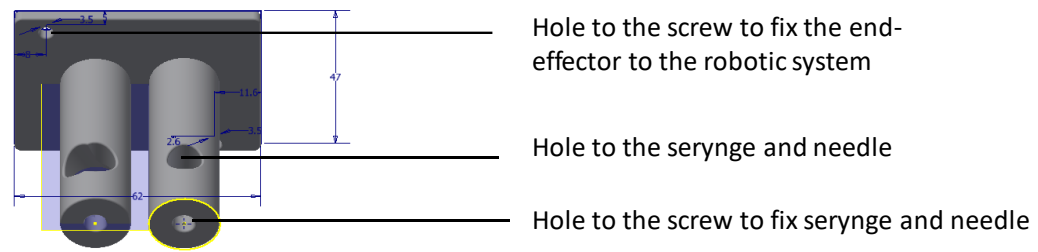
<b>Support of the electrodes</b>	<b>Support to fix the well plates</b>
Easy to couple to the cartesian robot	Adjusted to the specific dimensions of the well plates
Easy to put and remove the electrodes	Easy to couple to the cartesian robot's basis
Easy to adjust the specific position of the electrodes	

After several tests and modifications of the design of the parts, the final design of the pieces for the end-effector to support the needles and the support to fix the well plate in the basis of the system are presented in **Figure 13** and **Figure 14**.

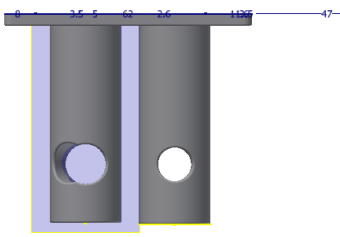
The design of the support for the well plates consisted of a frame with the dimensions of the plate to be fixed in the table of the mechanism (as analysed in the previous section). With this, the spatial coordinates of the wells can be defined in a fixed position.

Regarding the end-effector, the design of the piece consists of an area to insert the two needles, an area to tighten a screw to fix the needle and two holes to fix the end-effector to the robotic structure with screws.

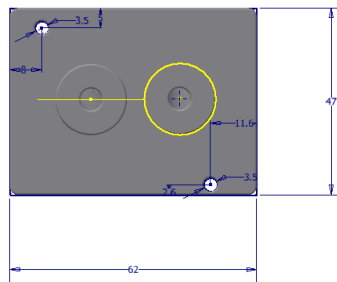
The designs were saved in the file type Standard Tessellation Language (STL) since in additive manufacturing, CAD files must be transpose to a language compatible with 3D printers. The models must be previously divided into layers for giving the useful information for the 3D printing machines. The main function of STL is precisely to divide the models into layers for the 3D printing machines [50]. For that, the slicer software used was Vertex 3D Printer Repiter Host, which converts the 3D models into instructions for 3D printing machines [48].



a

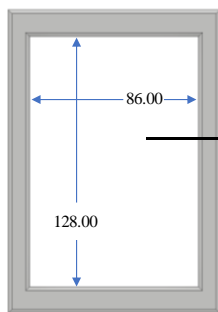


b



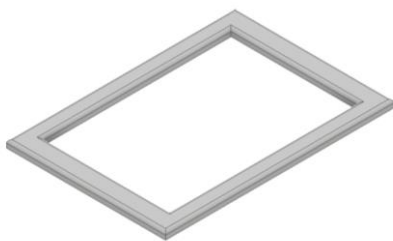
c

**Figure 13** – 3D draft of the piece for the support of the electrodes. **a:** oblique view; **b:** top view; **c:** front view.

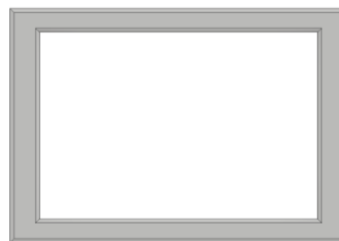


Area to fix the well plate in the basis of the robot mechanism

a



b



c

**Figure 14** – 3D draft of the support to fix the well plates in the basis of the robotic system. **a:** top view with the dimensions in millimetres; **b:** oblique view; **c:** top view.

As for the 3D printing material, the most common ones are polylactide (PLA) and acrylonitrile butadiene styrene (ABS), while polycarbonate (PC), nylon, polyethylene (PET) and thermoplastic elastomers (TPE) are not so common.

PLA, comparatively to ABS, is easier to use in the 3D printer and the results obtained are better, since it does not suffer significant distortions during the printing process, and it has a good adhesion to the platform of the 3D printer. ABS is more adequate for applications withstand high temperatures since it is a very resistant thermoplastic; PLA tends to deform at temperatures over 60 °C but this is not the case since the pieces are not exposed to high temperatures. Also, ABS is more ductile while PLA is more rigid, and for this study, the pieces are supposed to present a good tensile strength (more rigid) [48,51].

Taking this into account and considering the good mechanical properties, low price and moderate flexibility, PLA was the material selected to manufacture the pieces.

The mechanical properties of the pieces depend on the material (PLA) and on the specific parameters selected in the 3D printer slicer software. For the pieces developed, it was selected an infill density of 25% and the infill pattern grid. These parameters were selected taking into consideration previous studies that demonstrated to be suitable for the manufacturing of PLA pieces [48].

After the 3D printing, the pieces were assembled to the robot mentioned in section 3.2, to construct the system of application of CAP. The robotic system is presented in the following **Figure 15**.

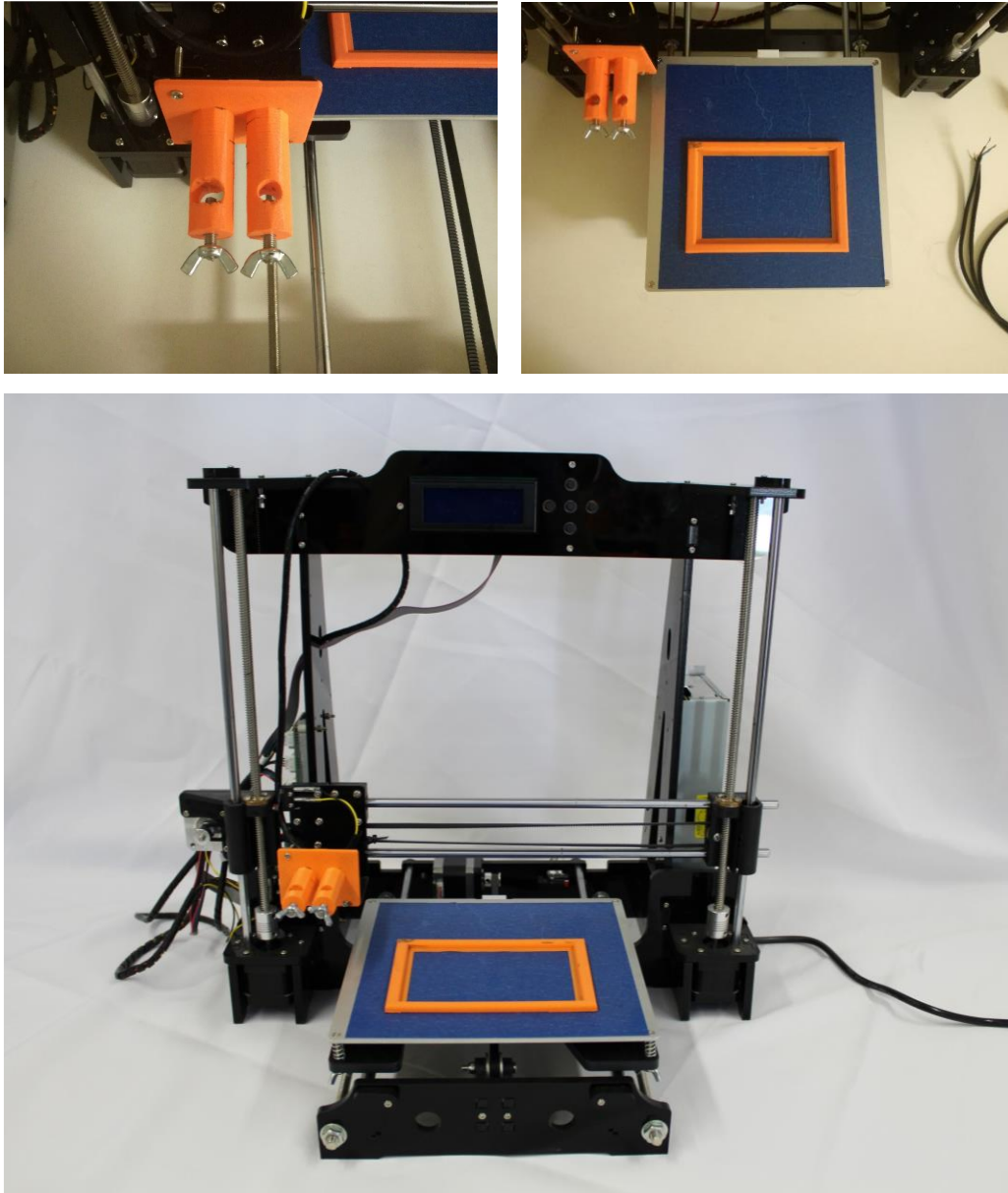


**Figure 15** – Robotic system developed.

The electrodes of the system need to be a conductor material and must be disposable and easy to change because of the application in different cell lines. The solution found was to use sterilized needles,  $30.9 \times 400$  mm, 5/8 (BD Microlance™, REF 301300), coupled to a syringe of 1 ml (*BD Plastipak™*, REF 303172, Spain), as it is represented in **Figure 16**.



**Figure 16** – Needle and syringe used as electrodes for CAP ejection.

The images of **Figure 17** illustrate the robotic system developed with the end-effector accoupled to the needles connected to crocodile electric plugs that are responsible for plasma conduction. In the basis of the robotic system is the well plate fixed with the support of the PLA piece. The images show how the system applies CAP in cell lines.

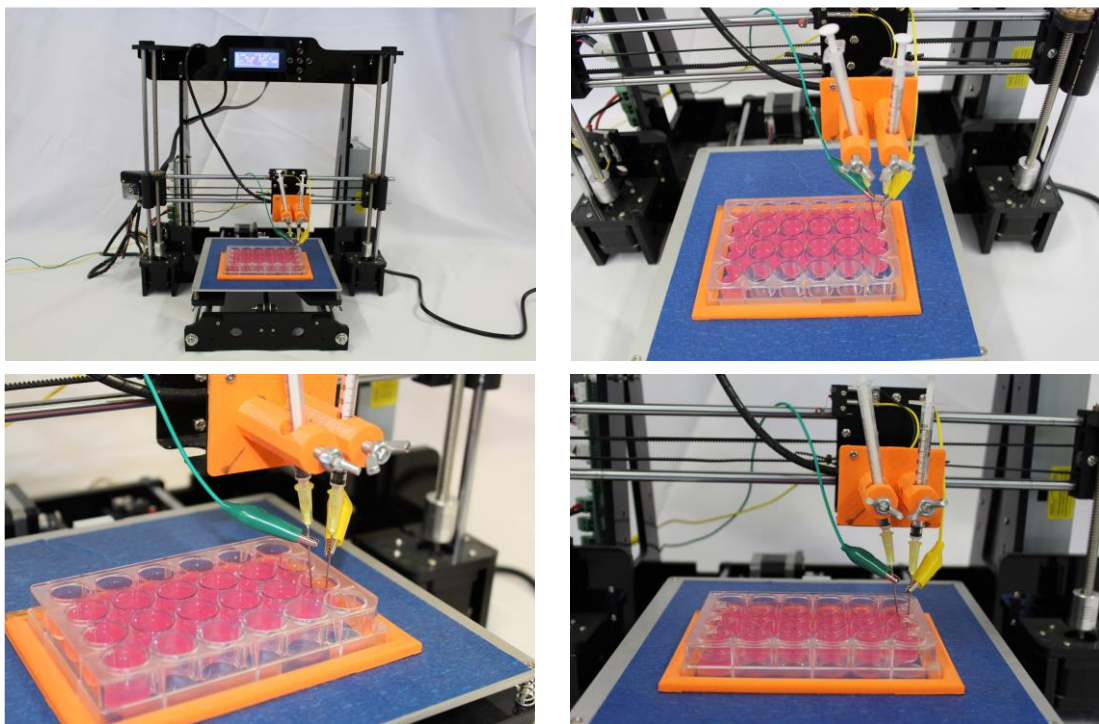


**Figure 17** – Scheme of the robotic system performing CAP application.





# Chapter 4: Human-Machine Interface

---

## 4.1 GRAPHICAL USER INTERFACE

This chapter describes the interface developed with the purpose of facilitating the interaction between the user and the robotic system.

The interface consisted of a user-friendly MATLAB GUI for personalized programming of the automatized system. The purpose of the GUI is to facilitate the researcher making use of the robotic system, by enabling any user to easily customize the application of CAP.

Until now, the CAP irradiation performed by the robotic system can occur in two types of well plates: 24 and 48-well plates (SPL Life Sciences Co., Ltd), as represented in **Figure 18**.

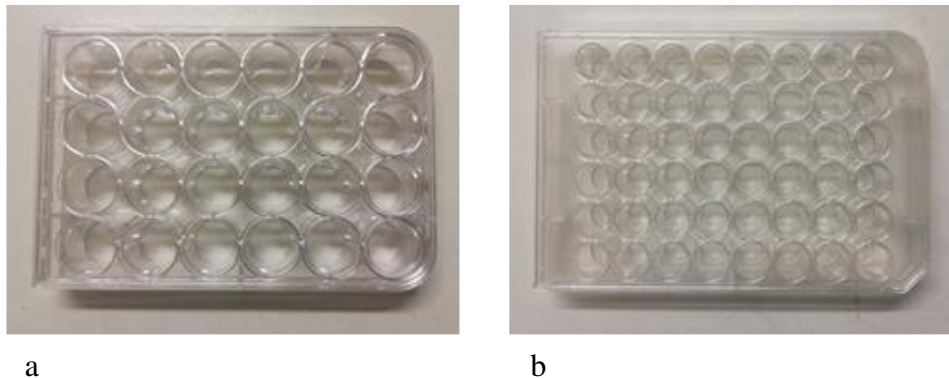


**Figure 18** – **a**: 24-well plate and **b**: 48-well plate for cell culture.

The wells of the 48-well plates are displaced in a matrix 6x8 with columns identified by numbers ranging from 1 to 8 starting in the left and lines identified by letters from A to F starting on top. The wells of the 24-well plates are displaced in a matrix 4x6 with columns identified by numbers ranging from 1 to 6 from left to right and lines identified by letters from A to D, starting from the top, as it is schematized in **Figure 19**.

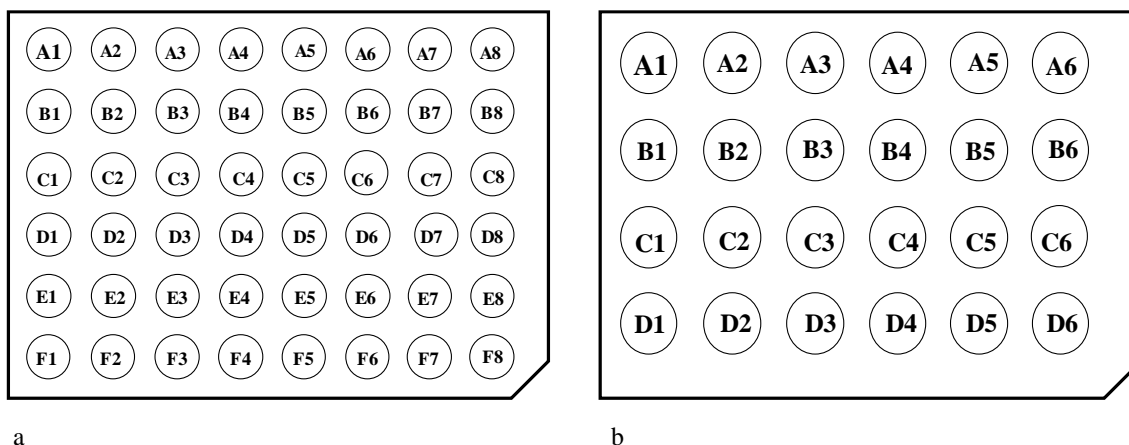


**Figure 19** – Identification of the wells of the multiwell plates, **a**: 48-well plate; **b**: 24-well plate.

The requirements identified for the GUI are the variables that the user is allowed to change: type of well plate to irradiate; which wells of the well plate are intended to irradiate; and irradiation time of each well.

The MATLAB software, version R2018b, was used to develop the GUI. The purpose was to create an intuitive interface, so, to design it, the App Designer MATLAB (ADM) tool was used (available since R2016 versions), because its environment enables an enhanced design and a large set of components for the user interface (UI) [52].

The ADM tool enables the combination of the organization of visual components and the programming of the interaction and behaviour of the App. App Designer generates object-oriented code allowing the programmer to easily add new properties, functions and callbacks, and the code is based in the MATLAB class structure. The code is constituted, first, by the App properties and, then, by the defined functions, the code and the components for the App initialization [52].

The GUI was transposed to a standalone application so that it can be used in any computer.

The interface enables any user to customize the system for a specific program of CAP irradiation. The user can select the well plate available to irradiate, between 24 and 48 well plates. The user can select which specific well or wells is/are intended to irradiate and, then, since the irradiation of CAP is time variable, it is also possible to choose the time of the irradiation individually for each well.

The programming of the movements of the linear motors of the robotic system were made in G-code, an intuitive programming language for robotic systems. A more detailed explanation of G-code language will be presented in section 4.2.

Each well is associated to spatial coordinates that are previously introduced manually in the software as a setup step. So, by selecting one well, the program will generate a G-code command to that specific coordinates. Then, the user can, manually, insert the pretended irradiation time per well, in milliseconds, since, in G-code, the time command must be inserted in milliseconds.

Schematically, an example of an interaction between the user and the system is represented in **Figure 20**.

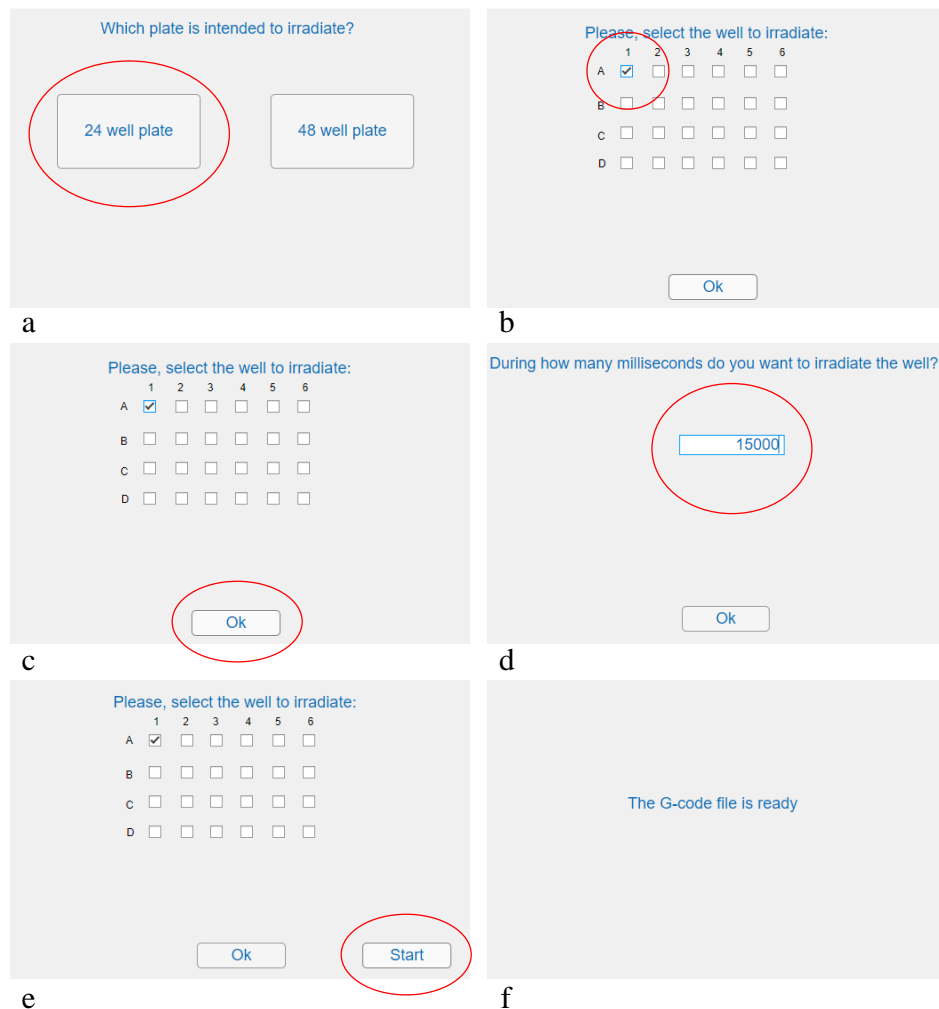


**Figure 20** – Scheme of an interaction. **a:** Selection of the well plate to irradiate (24 well-plate); **b:** Selection of the well to irradiate (well A1); **c:** “ok” button when the well is selected; **d:** Selection of the time to irradiate the well selected (15 seconds); **e:** If there is no more wells to irradiate, “Start” button is pressed; **f:** When “Start” button is pressed, a G-code file is returned.

In the subsequent image, **Figure 21**, there is a pseudocode algorithm schematizing the generation of the G-code file that the GUI returns.

---

**Algorithm 1** – Generation of G-code file for the robotic system

---

**Input:** Well plate, wells, irradiation time

**Output:** G-code file

```
1 Begin
2   If Well plate = 24
3     Select Well
4     For i = 1 to 24-well coordinates
5       If 24-well coordinates = well
6         G-code file.add 24-well coordinates;
7       End If
8     Select irradiation time;
9     G-code file.add irradiation time;
10    End For
11  If Well plate = 48
12    Select Well
13    For i = 1 to 48-well coordinates
14      If 24-well coordinates = well
15        G-code file.add 48-well coordinates;
16      End If
17    Select irradiation time;
18    G-code file.add irradiation time;
19    End For
20  End If
21 End
```

**Figure 21** – Pseudocode algorithm of the generation of the G-code file in the GUI.

## 4.2 NUMERICAL CONTROL

This section is meant to contextualize and explain how the cartesian robot is controlled. Numerical control (NC) or computer numerical control (CNC) is a mode of programmable automation in which coded alphanumeric data are used to control the actions and movements of an equipment. CNC is usually required for two different categories of applications: machine tooling (drilling, milling and turning) and non-machine tooling (assembly, drafting and inspection) [36].

Some of the main features of CNC are the ability to store and edit programs, programming subroutines, interpolation, communications interface and diagnostics. This allows CNC to have a very wide range of applications in many fields [36].

In the developed robotic system, alphanumeric data represent the relative positions between a workhead (the end-effector) and a workpart (the well plate), that is, the relative positions between the robot and the material of the application.

#### 4.2.1 G-CODE

G-code is the language used in CNC machines that contains the commands for the movements that must be performed. It is used to program and control the machine's movements by a compact code of commands and coordinates for the cartesian axes. The language commands are directed to the machine's motors and instruct the coordinates where to move, with which speed and the path to follow [53-54].

For this study, the control of the robot was made using G-code containing the linear moves for the end-effector to each specific position in each well. In G-code, the command responsible for linear moves is "G0", and the coordinates were defined to be in absolute positioning relatively to the origin, which, in this case, is the left-hand corner of the basis of the system. For the spatial coordinates of X, Y and Z axes, corresponding to the position of the wells in the well plate, the units are in millimetres.

The irradiation time is defined as the time that the electrodes need to be positioned in each well. The command used in G-code is "G04" and the time is introduced in milliseconds.

To allow the correct generation of a G-code for each specific case of irradiation, a support was built, in order to fix the plate in one position of the basis of the robotic system, as explained in the previous **chapter 3**. With this, it becomes possible to manually define the spatial coordinates of all wells. In this way, the coordinates of the wells in the well plates were introduced and saved in the MATLAB application. Consequently, when the user selects the wells individually, the coordinates are automatically associated to the chosen wells.

For example, if the objective is to irradiate cells in the well of the position A1 of a 24 well plate for 15 seconds, which is the case of the interaction in **Figure 20**, the return of the interface would be a file containing the following G-code:

```
G28 (1)
G0 X35 Y180 Z70 (2)
G0 X35 Y180 Z30 (3)
G04 P15000 (4)
G0 X35 Y180 Z70 (5)
G28 (6)
```

The explanation of the code lines is as follow.

(1) Command to move all the axis to the origin (0,0,0) mm.

(2) G0 is the command to the linear movement, in this case, from the origin to the point of coordinates (35,180,70) mm. The X and Y coordinates correspond to the position of A1 well of the 24-well plate, and Z coordinate is a distance that prevents the electrodes connected to the end-effector from touching the well plate.

(3) The command is responsible for the movement from the preceding position (35,180,70) mm to the new position, and as this command only contains information for the Z axis, and X and Y remain with the same coordinates. The new position is then (35,180,30) mm that corresponds to the position where the electrodes are inside the A1 well of the 24-well plate.

(4) The command G04 is the command used to pause the program during the time specified in P command, in milliseconds. In this case, the end-effector stops in the aforementioned position for 15 seconds, that is the time for the CAP irradiation.

(5) After the pause for the CAP irradiation, the electrodes rise to a position out of the wells to continue the program with linear moves without hitting the plate.

(6) When the program ends, all the axes are moved to the origin, using G28 command.

CAP discharge occurs whenever one electrode is placed inside the medium containing the cells, and the other above the surface of the medium. So, for this reason, the CAP production device is always switched on during the performance of the

technique. Thus, when the electrodes are in the correct position for the discharge, CAP is irradiated.

Following is presented a use case that illustrates how the user interacts with the system and what the system does automatically (**Figure 22**), for a better understanding of the process.

A business process model was designed using the Business Process Model and Notation 2.0 (BPMN 2.0) scheme, in order to represent the whole process involved in the technique of CAP application performed manually (**Figure 23**) and performed with the robotic system (**Figure 24**).

BPMN is commonly used to describe a business process. In this case, the process is the technique of CAP application in cell lines. The schemes present the responsible for each activity, the relation between them, possible options, decisions taken during the procedure and everything that is automatically done [55].

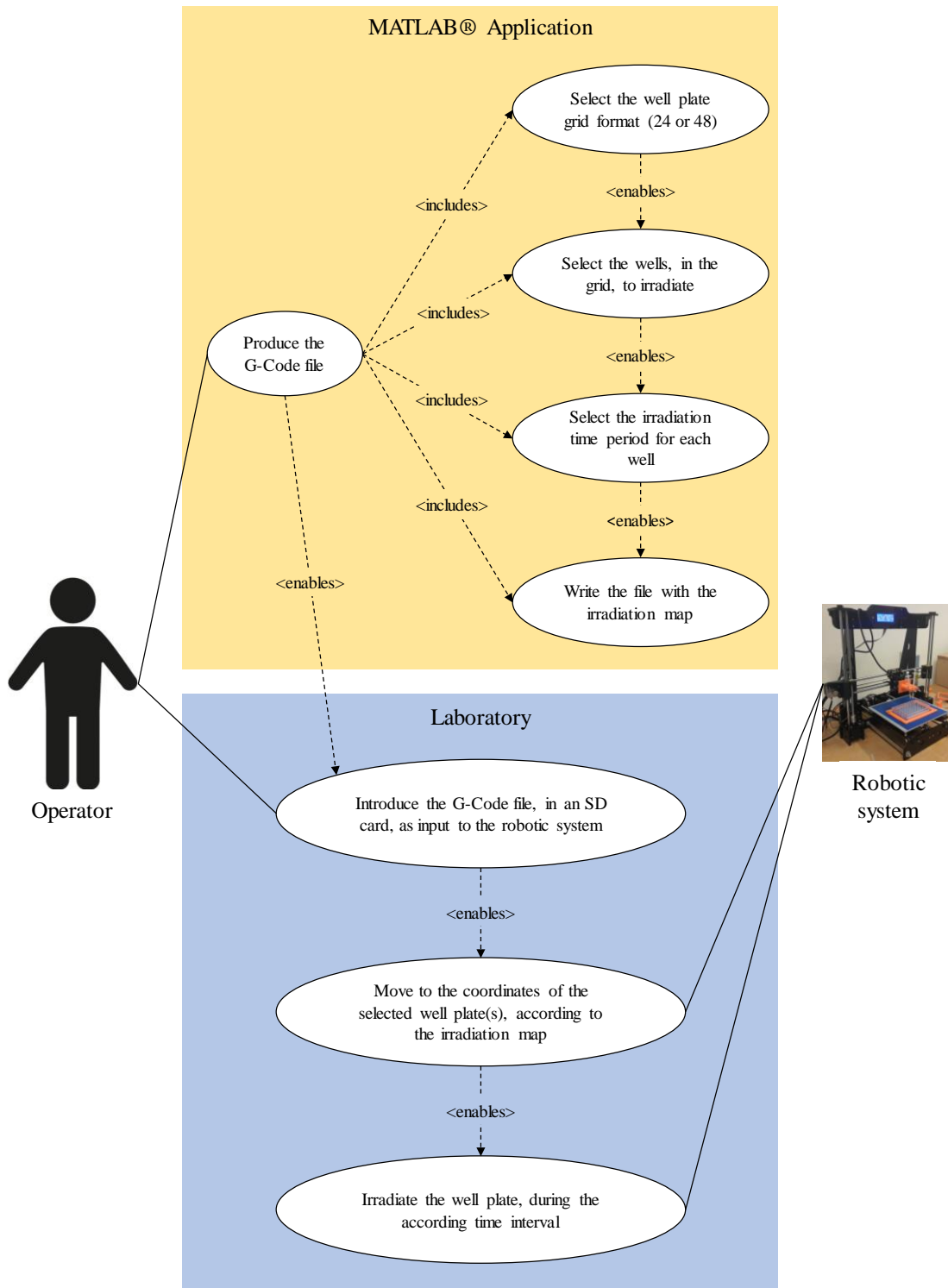


**Figure 22** – Use Case scheme of the interaction between the user and the system.





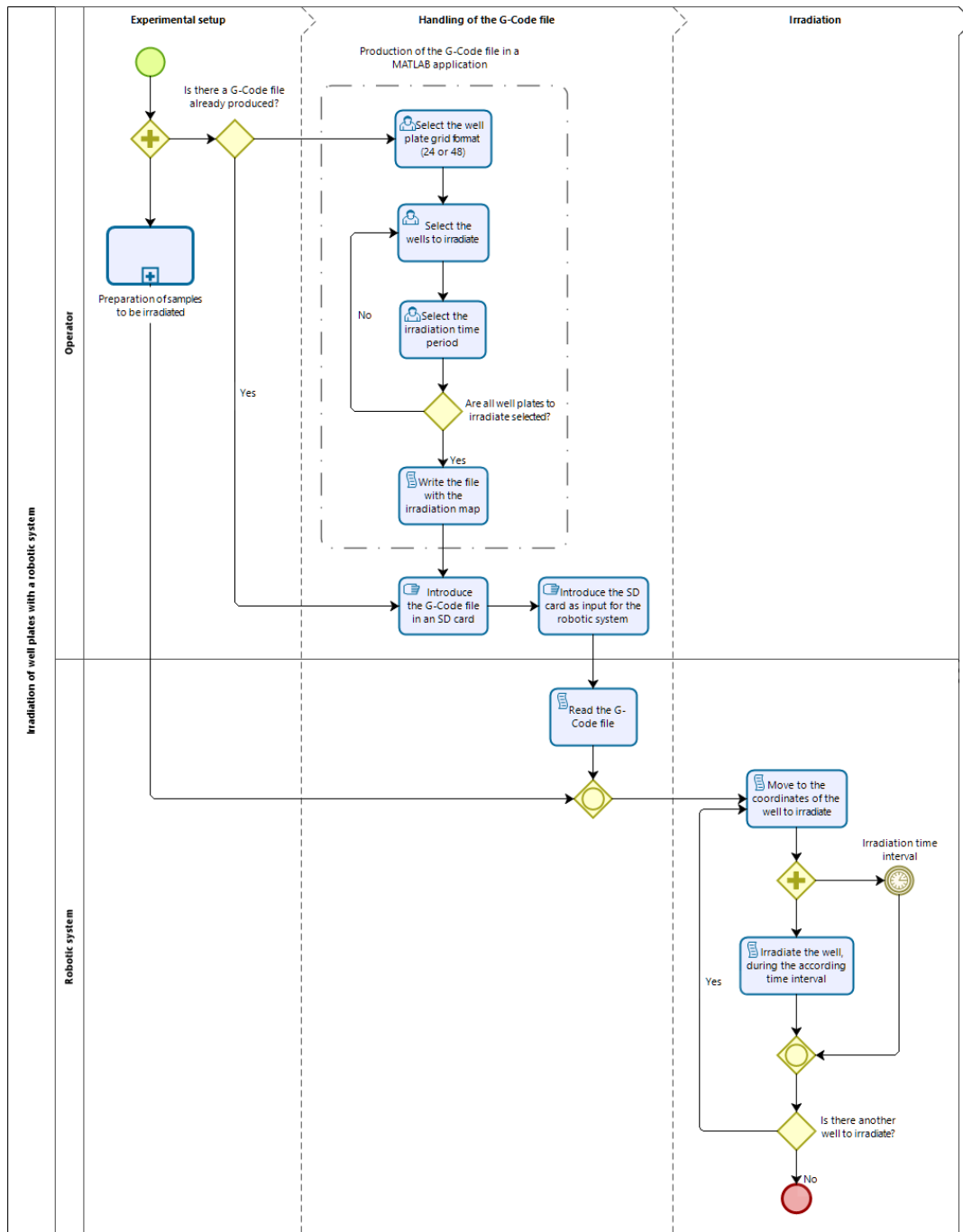


**Figure 24** – Model of the process of CAP application with the robotic system.

# Chapter 5: Procedures

---

This chapter describes the protocols of cell culture and viability tests performed after irradiation of CAP to study its influence in endometrial cancer and evaluate the robotic solution developed.

## 5.1 CELL CULTURES

All the procedures involving cell manipulation were performed in fully equipped cell culture rooms at Biophysics Institute, Faculty of Medicine in the University of Coimbra, Portugal.

For the studies *in vitro* of endometrial cancer, three different cell lines were used: ECC-1 and RL-95 – acquired from the American Type Culture Collection (ATCC), USA – and Hela (gently characterized and given by the University of Campinas, Brazil). The three cell lines are tumor cells from the human endometrium tissue.

All the procedures concerning cell handling were performed using lab coat and gloves. Live cells were always manipulated inside a laminar flow chamber (Faster BH-EN 2004). Every used material was vaporized with alcohol at a concentration of 70% before being placed inside the laminar flow chamber to ensure that the conditions are sterilized.

The three cell lines were defrosted strictly following the protocol given by the provider. The cells were maintained in culture in an incubator (Binder, *Dias de Sousa S.A Portugal*) at 37°C, with an atmosphere of 95% of air and 5% of CO<sub>2</sub>.

Hela and RL-95 cell lines were maintained in 75 cm<sup>2</sup> cell culture flasks (SPL Life Sciences Co., Ltd, Korea) containing the culture medium Dulbecco's Modified Eagle's Medium (DMEM) (Sigma D-5648-50L), supplemented with 5% of Fetal Bovine Serum (FBS) (Sigma F7524). For ECC-1, the medium culture was Roswell Park Memorial Institute 1640 Medium (RPMI) (Sigma R4130-50L), supplemented with 5% of FBS, also in 75 cm<sup>2</sup> cell culture flasks. Cells were maintained in culture

conditions and the medium was changed every two days until they were 70-80% confluent and ready for being transferred to perform the assays.

The three cell lines were photographed in normal conditions, using a microscope (Motic, MoticamPro-285A, AE31) with 100x magnification, **Figure 25**.

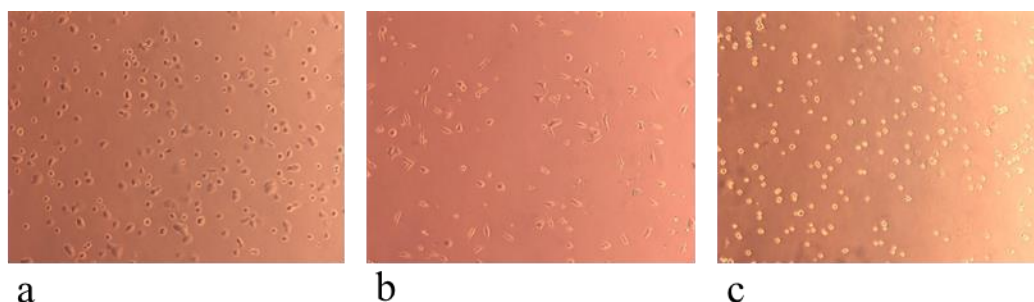


**Figure 25** – Cell lines in culture, **a:** ECC-1 cells; **b:** HeLa cells; **c:** RL-95 cells.

## 5.2 COLD ATMOSPHERIC PLASMA IRRADIATION

Cells were irradiated with CAP in 48-well plates (Costar<sup>®</sup>, Corning Incorporation, 3548) at a concentration of  $2.5 \times 10^5$  cells/mL with 200  $\mu$ L/well. The assays were performed using multiwell plates in which cells were distributed, allowing culture cells to maintain equal conditions in every well.

To transfer cells from the cell culture flask to 48-well plates, it was necessary to detach the cells from the surface of the cell culture flask, and for that, the culture medium was firstly aspirated and, then, the flask was washed with 4 mL of Phosphate-buffered saline (PBS) – 137 mM NaCl (S7653, Sigma, USA), 2.7 mM KCl (P9333, Sigma, USA), 10 mM  $\text{Na}_2\text{HPO}_4 \cdot 2\text{H}_2\text{O}$  (S5011, Sigma, USA) and 2 mM  $\text{KH}_2\text{PO}_4$  (P0662, Sigma, USA), pH=7.4. Then, the supernatant was aspirated again. Cells were incubated at 37 °C during 5 minutes with 2 mL of trypsin-EDTA at 0,25% (Sigma T4049), which is a protease responsible for cell detachment.

To inactivate trypsin, 4 mL of medium (DMEM or RPMI) were added and, using a pipette, cells were suspended and transferred to a 25 mL falcon tube. Then, it was necessary to count the cells in order to calculate the quantity of solution needed to

obtain a concentration of  $2.5 \times 10^5$  cells/mL. Using a pipette, a small quantity (around 40  $\mu\text{L}$ ) of solution was transferred to an Eppendorf that was then placed outside the laminar flow chamber. In a new Eppendorf, 20  $\mu\text{L}$  of the solution containing cells and 20  $\mu\text{L}$  of trypan blue (Sigma-Aldrich, T0776, USA) – a dye responsible for distinguishing living from dead cells – were pipetted. Then, the cell suspension was homogenized and it was proceeded to cell count in the Neubauer Chamber (Neubauer-improve, 0640030, Germany), through a microscope with magnification of 40 x. The Neubauer Chamber is composed by four quadrants, as it is schematized in **Figure 26**, and for each quadrant, the volume considered is  $1 \times 10^{-4}$  mL, thus, the number of cells in 1 mL is given by **Equation 3**.

$$N = C \times D \times 10^4 \text{ cells/mL} \quad (3)$$

Where,  $C$  is the Number of cells counted in one quadrant divided by the means of the cells counted in the four quadrants, and  $D$  is the Dilution factor.

For cell counting, the Chamber was centred in the microscope, one quadrant at each time, and the cells of that quadrant were counted. The quadrant has four sides, limited by a line, therefore cells counted are the ones inside the quadrant and touching half of the border lines, as it is represented in **Figure 26**.

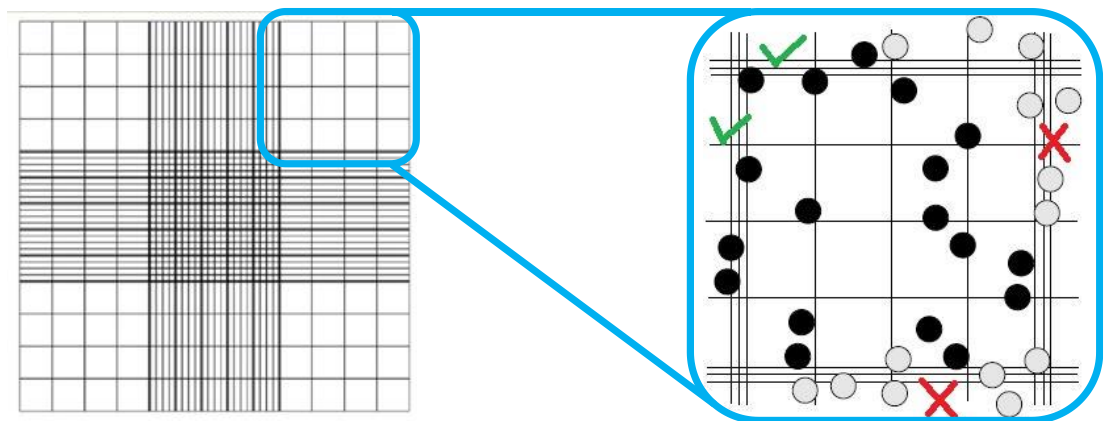


**Figure 26** – Neubauer Chamber scheme (adapted from [56]).

As already mentioned, for the CAP irradiation, the concentration per well must be  $2.5 \times 10^4$  cells/mL and the volume per well (200  $\mu\text{L}$ ). The final volume can be

estimated multiplying the number of wells to irradiate by the volume per well (200). In this way, the volume needed is calculated by **Equation 4**.

$$C_i \times V_i = C_f \times V_f \quad (4)$$

$$V_i = \frac{C_f \times V_f}{C_i}$$

Where,

$$C_i = N \text{ cells/mL},$$

$$C_f = 2.5 \times 10^4 \frac{\text{cells}}{\text{mL}},$$

$$V_f \approx 200 \times (\text{number of wells to irradiate}) \text{ mL}.$$

After this procedure, the value obtained for the initial volume was transferred to a new falcon tube using a pipette. Considering that  $V_f > V_i$  (otherwise the experiment is invalid due to the small number of cells), using a pipette, the falcon was filled with a volume of  $V_f - V_i$  of culture medium, so that the final volume could be obtained with the desired concentration. Finally, the wells of the 48-well plate to irradiate were filled with 200  $\mu\text{L}$ .

The cells were maintained in the incubator overnight to allow them to adhere to the surface of the plate and, then, CAP irradiation was performed.

For this study, CAP irradiation was performed for 15, 30, 60, 90 and 120 seconds. Control wells, which were not irradiated, were produced in every experiment. Every experiment was performed in triplicate. **Figure 27** shows one multiwell plate containing ECC-1 cells with 3 wells prepared for each irradiation time.

CAP irradiation was performed manually and with the developed robotic system. Manual CAP application is described in **chapter 2**, and robotized CAP application technique is described in **chapter 4**.

For the programming of the robotic system, the GUI was used, and the parameters chosen for all the performed assays were equal: 18 wells of a 48 well plate, displaced in a matrix 3x6 (see **Figure 27**), where three wells were the control, three were to irradiate during 15 seconds, three during 30 seconds, three during 60 seconds, three during 90 seconds and three during 120 seconds. Also, for the calibration of the

specific position for the CAP discharge, a well to be discarded was used as a reference well to calibrate the position (this was the well in position A7).

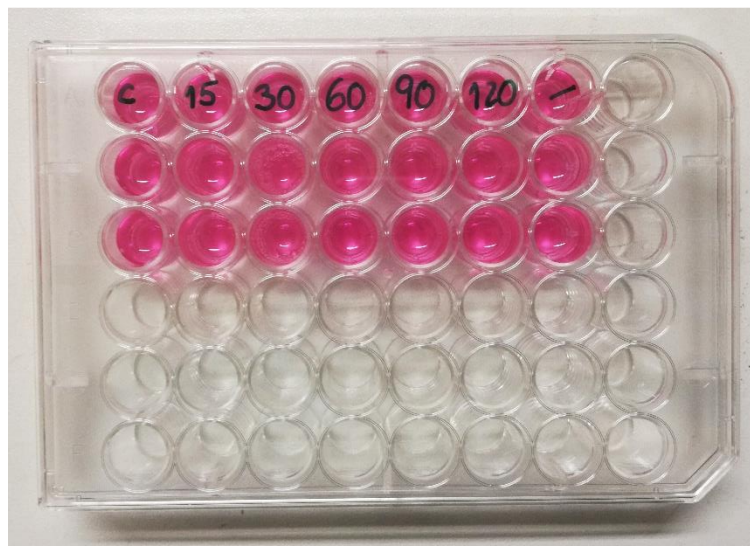


**Figure 27** – 48-well plate identified containing ECC-1 cells for CAP irradiation.

### 5.3 VIABILITY ASSAYS

After CAP irradiation, cells were left at 37°C in the incubator for 24 hours and, after this period, viability tests were performed in order to evaluate the influence of CAP irradiation in cell viability. The performed assays were Sulforhodamine B (SRB) and MTT (3-(4,5-dimethylthiazol-2-yl)-2,5-diphenyltetrazolium bromide).

#### 5.3.1 MTT

To evaluate the effect of CAP irradiation in the metabolic activity of cells, the MTT assay, a colorimetric test, was performed.

MTT is reduced by metabolically active cells, in the presence of NADH, resulting in formazan crystals (**Figure 28**). Formazan crystals present a dark purple colour, with a maximum of absorbance of 570 nm, which can posteriorly be quantified by spectrophotometry [57]. The lower the value obtained in the spectrophotometer, the

lower the MTT reduction, corresponding to a minor cell viability. This method is, thus, an indirect way of evaluating mitochondrial function – the quantity of crystals formed is directly proportional to the quantity of metabolically active cells [58].

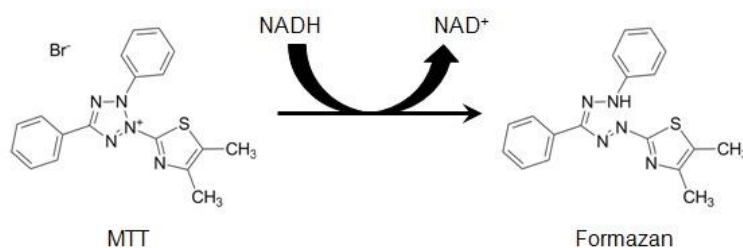


**Figure 28** – Structure of MTT and Formazan [59].

To perform the MTT assay, the well plates containing the cells were, firstly, washed with PBS. Then, 100  $\mu$ L of a solution of MTT (Sigma M5655, USA) at 5 mg/mL with a pH at 7.4, was added in each well. Incubation was performed at 37° C, during 4 hours, which is the minimum time to form all the Formazan crystals.

After the 4 hours of incubation, the crystals were solubilized. For this, each well was filled with 100  $\mu$ L of a solution of 40mM hydrochloric acid (HCL) (100317, Merck Millipore, USA) in isopropanol (278475, Sigma, USA), and the plates were agitated during approximately 20 minutes.

The contents of the well were, then, transferred to a 96-well plate to quantify the absorbance of the samples at 570 nm and 620 nm, using the spectrophotometer (Biotek® Synergy HT, USA).

### 5.3.2 SULFORHODAMINE B

SRB is the assay performed to evaluate cell viability via protein synthesis. SRB is a purple colour dye with affinity to bind to basic amino-acid residues in acidic conditions (**Figure 29**) and can be extracted in basic environment [57,60].



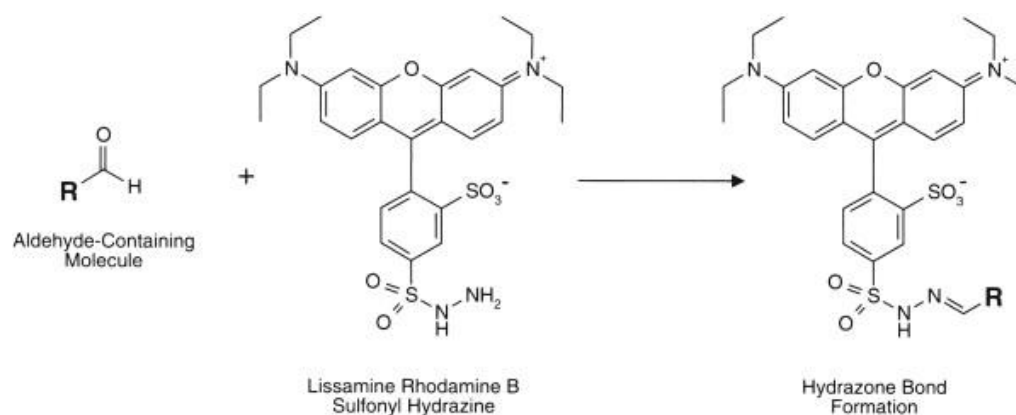


**Figure 29** – SRB structure and interaction (adapted from [61]).

To perform this assay, the well plates were washed with PBS and left to dry at room temperature. Using a pipette, it was added 200  $\mu$ L of 1% acetic acid (Sigma 109088, USA) in methanol (Sigma 322415, USA) in each well. Plates were incubated at 4  $^{\circ}$ C for 1 hour. The methanol was discarded, and the well plates were left to dry at room temperature.

The next step was to add 200  $\mu$ L of a solution of 0.4% SRB (Sigma S9012, USA) in each well and incubate in the dark, at room temperature, for, approximately, 90 minutes. Afterwards, the well plate was washed with water to remove the excess of SRB and then the plate was left to dry at room temperature. After this, 200  $\mu$ L of TRIS-NaOH at pH = 10 (T1503, Sigma, USA) were added with a pipette in each well. Subsequently, the solutions were transferred to a 96-well plate, to read the absorbance values in a spectrophotometer (Biotek® Synergy HT, USA), at wave-length of 540 nm and with a reference at 690 nm.

## 5.4 STATISTICAL ANALYSIS

Results were primarily treated using Excel software. The difference between the two absorbances, at 570 and at 620 nm, obtained in the spectrophotometer was calculated, and the results were normalized to the control cultures.

With the normalized results from both viability assays, boxplots were constructed for each case study of CAP irradiation, using Graphpad Prism 5 software. The results were plotted in reference to the control that was not irradiated with CAP.

Thereby, for the SRB assay, control cells presented 100% of protein content and, for the MTT assay, 100% of metabolic activity. Cell death is assumed to be a direct consequence of CAP irradiation.

Each boxplot was constructed with the results of several experiments ( $n=9$ ) with the same conditions, which is a result of several procedures, including cell culture maintenance, CAP irradiation and viability assays, so, it must be considered that the variability of the results can be affected by several factors associated with the procedures. Temperature, cell responses, reagents, procedure laboratory techniques and unidentified cell or reagents contaminations represent some of the aspects that can suffer changes and influence the results, despite all the protocols being performed with the maximum rigor.

The statistical analysis was performed using the SPSS Statistics Software (Version 25), from IBM Corporation. To compare the cellular viability between the irradiation times tested, the non-parametric test Kruskal-Wallis was performed. Besides, to compare percentual values of cellular viability between specific CAP irradiation times, the Bonferroni test was performed. It was considered that statistically significant differences are determined by  $p < 0.05$ .

To compare the variability between the manual and robotic CAP application techniques, using the SPSS Software (Version 24), it was determined the coefficient of variation,  $CV = \frac{s}{\bar{x}} \times 100\%$ , with  $s = Standard\ Deviation$  and  $\bar{x} = Mean$ , of the obtained values of protein content and metabolic activity. The  $p$  values were also obtained, through the Levene test. The variability was considered statistically significant when  $p < 0.05$ .

In order to evaluate any possible interference and influence of the robotic system on the results, the variability of all the obtained results was analysed.

In a boxplot, the dispersion of the data can be represented by the interquartile range of the boxplot, and this is the more robust statistic to measure the variability of the results, since it is not affected by outliers [62]. The coefficient of variation was also analysed to evaluate and compare the variability between obtained results with manual and robotized CAP application.

## 5.5 POSITION ERROR OF THE ROBOT

In order to test and validate the accuracy of the robotic system, measurement tests were performed to calculate the error associated with the three linear motors of the system.

As mentioned in **chapter 3**, section 3.1.1, the accuracy of the linear motors of the system, defined by the seller, is 0.012 mm for X and Y axes and 0.004 for Z axis. Yet, after constructing the robotic system, tests were performed to calculate and validate the position error of the linear motors of the system.

To achieve that, a sequence of 20 repetitions of a linear movement of 20 mm was programmed in G-code, for each of the 3 motors, as it is represented in **Figure 30**. Using a digital caliper, the values were manually measured and registered.

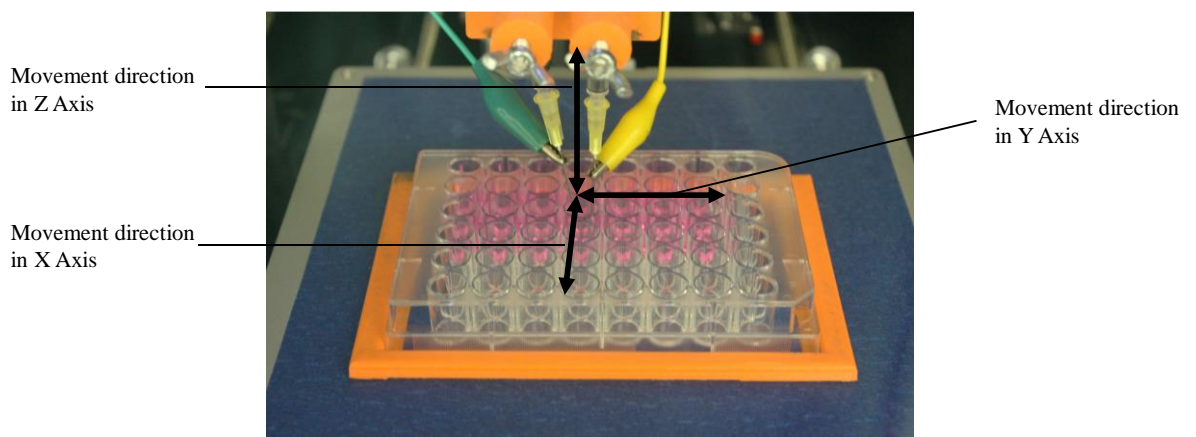


**Figure 30** – Scheme of the movements for the measurements.

For the values of X and Y axis, the measurements were registered including the value of the electrode diameter, which corresponds to the needle diameter. This value can be considered as a systematic error, so, for the calculation of the error, it can be subtracted to the total measurement:

$$\textit{Electrode Diameter} = 1.00 \pm 0.01 \textit{ mm}$$

Hence, in all the measurements made in the X and Y axis, the value of 1 mm is subtracted, corresponding to the diameter of the electrode.

The value of the full width at half maximum (FWHM) (**Equation 5**) was considered as the reference value to characterize the position error of the robotic system, since it is widely assumed that errors follow a Gaussian distribution and it is expected to have approximately 68% of the variation within half of the maximum amplitude measured. Therefore, this value is commonly used to reflect resolution, and it respects the following equation:

$$\text{FWHM} = 2.35 \text{ s} \quad (5)$$

With,  $s$  = standard deviation.

# Chapter 6: Results and Discussion

---

## 6.1 ACCURACY OF THE ROBOTIC SYSTEM

As presented in **Table 5**, the values of the mean and standard deviation of the measures were calculated for each of the axes X, Y and Z, in order to evaluate the position error of the robotic system.

For the X axis, results are as follows.

$$\text{Standard deviation}_{X \text{ axis}} = s = 0.059 \text{ mm}$$

$$\text{FWHM} = 0.13865 \text{ mm}$$

In **chapter 2**, section 2.1, it was established that the minimum limit for the accuracy of the system is 2.75 mm. Taking this into account, and comparing the value obtained for the position error, the relation between the obtained value and the reference value for the accuracy is as follows.

$$\frac{\text{FWHM}}{\text{Accuracy}} \times 100\% = \frac{0.13865}{2.75} \times 100\% \cong 5.04 \%$$

Considering the relation calculated above, it can be observed that the value obtained for the position error of the X axis of the robotic system constructed corresponds to, approximately, 5% of the accuracy established for the system, which means that the position error obtained for the X axis is adequate for the requirements of the system.

For the Y axis, the calculated results are as follows.

$$\text{Standard deviation}_{y \text{ axis}} = s = 0.047 \text{ mm}$$

$$\text{FWHM} = 0.11045 \text{ mm}$$

$$\frac{\text{FWHM}}{\text{Accuracy}} \times 100\% = \frac{0.11045}{2.75} \times 100\% \cong 4.06 \%$$

For the Y axis, the analysis of the measurements was the same as for the X axis. Analysing the relation between the FWHM and the accuracy calculated in **chapter 2**, it can be concluded that this axis is in conformity with the established value, since the value obtained for FWHM is, approximately, 4% of the value of the accuracy previously calculated. This means that the position error associated with the Y axis is acceptable, since it is contained in the value of the accuracy calculated as a reference (2.75 mm).

Lastly, for Z axis, the obtained results are as follows.

$$\text{Standard deviation}_{z \text{ axis}} = s = 0.031 \text{ mm}$$

$$\text{FWHM} = 0.07285 \text{ mm}$$

$$\frac{\text{FWHM}}{\text{Accuracy}} \times 100\% = \frac{0.07285}{2.75} \times 100\% \cong 2.64 \%$$

The treatment of the data was performed in the same way that for both X and Y axes, and in this case, the obtained value of FWHM is around 2% of the reference value (2.75 mm). Once more, this value is contained inside the limit value for the accuracy established in **chapter 2**, so, it can be considered adequate for the application.

After these tests were performed, it could be concluded that the robotic system has a position error smaller than the reference value of 2.75 mm for all the three axes. So, for the performance of CAP irradiation, the developed automatic system could be used assuring a good accuracy.

**Table 5** – Values of the measurements of the movements of the axes of the system.

	<b>X axis (mm ± 0.01)</b>	<b>X axis corrected (mm ± 0.01)</b>	<b>Y axis (mm ± 0.01)</b>	<b>Y axis corrected (mm ± 0.01)</b>	<b>Z axis (mm ± 0.01)</b>
1	21.04	20.04	21.10	20.10	19.98
2	21.18	20.18	21.00	20.00	19.98
3	21.00	20.00	21.07	20.07	19.99
4	21.05	20.05	21.01	20.01	20.00
5	20.94	19.94	21.10	20.10	20.04
6	21.00	20.00	21.00	20.00	20.00
7	21.00	20.00	21.00	20.00	20.01
8	21.02	20.02	20.96	19.96	20.00
9	21.04	20.04	20.90	19.90	19.94
10	20.99	19.99	21.10	20.10	20.00
11	20.89	19.89	19.99	19.99	20.04
12	21.00	20.00	21.04	20.04	20.01
13	21.11	20.11	21.00	20.00	20.00
14	21.05	20.05	21.00	20.00	20.00
15	21.01	20.01	21.01	20.01	19.94
16	21.02	20.02	21.02	20.02	20.01
17	21.00	20.00	20.94	19.94	19.95
18	20.96	19.96	21.01	20.01	20.06
19	20.98	19.98	21.00	20.00	20.04
20	21.00	20.00	21.03	20.03	20.00

## 6.2 RESULTS AND DISCUSSION OF THE APPLICATION OF CAP

This section includes the comparison between the results obtained with the manual and the automatic application of CAP in cell lines, in order to evaluate if the use of the robotic system influenced the results and to validate the developed system.

### 6.2.1 VALIDATION OF THE ROBOTIC SYSTEM

For the validation of the robotic system, the variability of all obtained results was analysed. For ECC-1 cell line, the values of metabolic activity and protein content, after manual and automatic CAP application, are illustrated in the graphs of **Figure 31**.

Protein content graphs are illustrated in **Figure 31-a** and **Figure 31-b**. First, for 15 seconds of irradiation, in manual CAP application, the interquartile range of the boxplot goes from 30% to, approximately, 75% of protein content, while for the irradiation with the robotic system, the results present a dispersion in a smaller range, from, approximately, 60 to 80% protein content.

For 30 seconds CAP irradiation time, with the robotic system, corresponding to **Figure 31-b**, the boxplot presents an interquartile range approximately between 30 and 55% of protein content, while in manual CAP application, represented in **Figure 31-a**, the dispersion of the boxplot, corresponding to the size of the box of the boxplot, is between 20 and 50% of protein content.

Then, for 60 seconds of irradiation with CAP, the variability of the boxplot resultant of the automatized CAP application (**Figure 31-b**), goes from, approximately 15 to 55%, while in the analogous results for manual CAP application go from 15 to 65% of protein content.

For 90 seconds CAP irradiation, both the red and the green boxplots present a similar variability of, approximately, 15 to 35% of protein content.



Lastly, for 120 seconds of CAP irradiation time, the interquartile range of the boxplot of the manual CAP application varies from 10 to 35% protein content and for the irradiation with the robotic system, the variability of the boxplot is from, approximately, 10 to 20% protein content.

For all the irradiation times compared, the interquartile range of the boxplots resulting from the automatic CAP irradiation is smaller than the boxes from the results of manual CAP irradiation. In every case, it can be visually seen that the interquartile ranges of manual and robotized CAP application intersect in the values of protein content for the tested times. In other words, the variability of the results corresponding to the robotized CAP application, illustrated in **Figure 31-b**, is contained in the range of variability of results corresponding to the manual CAP application, illustrated in **Figure 31-a**, for the same CAP irradiation time. This means that, despite the variability of results being different, the tendency of the results is similar, and this can be associated to the hypothesis that the robotic system reduces the variability without influencing CAP effects in cells.

In the case of the results of MTT assay for ECC-1 cell line, represented in **Figure 31-c** and **Figure 31-d**, the same analysis made for SRB results can be performed.

The boxplot corresponding to the manual CAP application, illustrated in **Figure 31-c**, considering 15 seconds of CAP irradiation, presents an interquartile range from, approximately, 20 to 60% of metabolic activity while, also for 15 seconds CAP exposure, the boxplot corresponding to the irradiation with the robotic system, represented in **Figure 31-d**, presents an interquartile range that varies from 65 to 80% of metabolic activity, approximately. In this case, the difference in variability is evident, but, despite the range between the maximum and the minimum values of the boxplot intersecting in protein content values, the interquartile ranges of the two boxplots do not intersect in any point, so, it is not appropriate to take conclusions about the robotic system based in these results.

Regarding the 30 seconds of CAP irradiation time, the variability of the boxplot corresponding to the manual CAP application varies from 5 to 45% of metabolic activity, approximately, whereas the variability of the boxplot corresponding to automatic CAP application varies from 20 to 35% of metabolic activity, approximately. In this case, the interquartile ranges of both boxplots coincide in the metabolic activity interval, since the interquartile range of the boxplot considering

robotized CAP application is contained in the interquartile range of the boxplot considering manual CAP application. This means that, despite the variability of the results obtained with the robotic system being much smaller than the ones from the manual CAP application, these data are correlated and consistent.

For the case of CAP irradiation time of 60 seconds, while for the manual CAP application the boxplot presents a variability from, approximately, 5 to 20% of metabolic activity, in automatic CAP application, the boxplot presents a variability from 3 to 15%, approximately.

For both 90 and 120 seconds of CAP irradiation times, the variability of results is similar for both plots – manual and robotized CAP application (corresponding to **Figure 31-c** and **Figure 31-d**, respectively) – and varies from, approximately, 3 to 10% of metabolic activity.

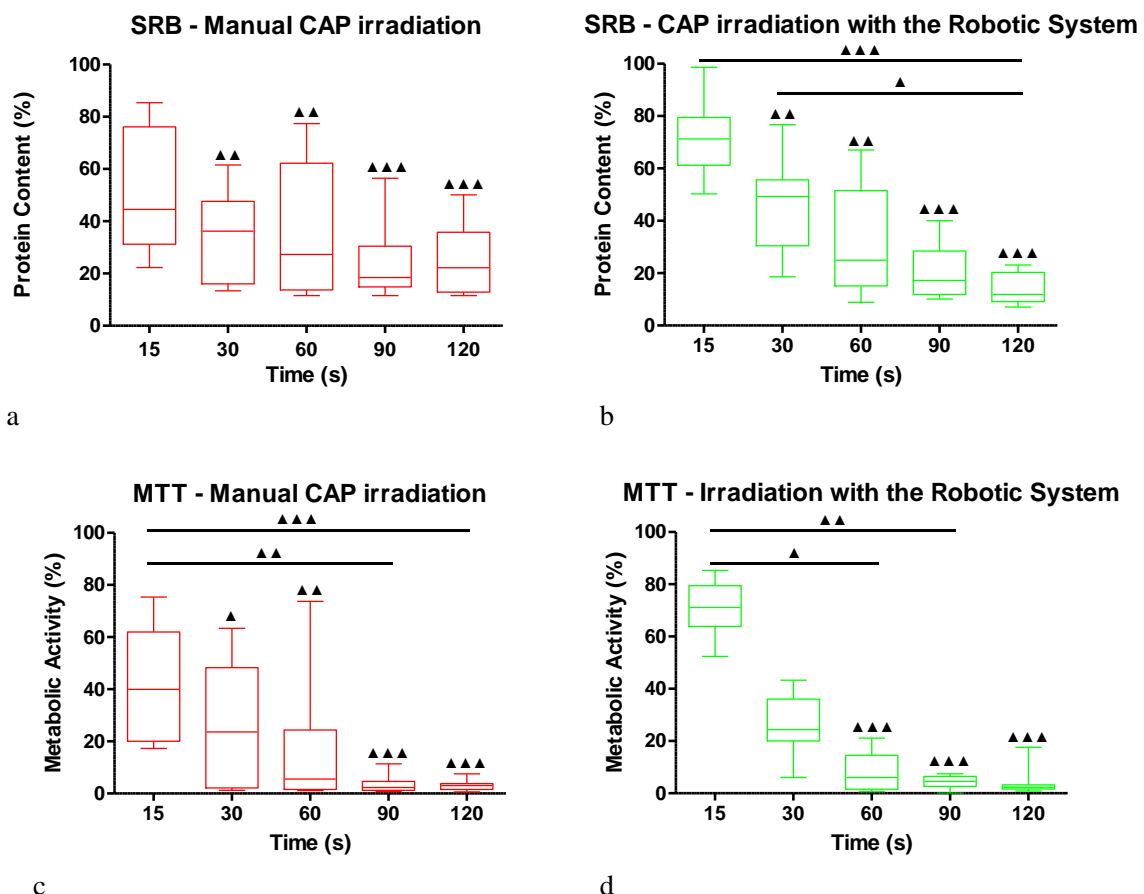


**Figure 31** – Boxplots of the results of the viability assays performed after ECC-1 CAP irradiation. **a**: SRB assay performed after manual irradiation; **b**: SRB assay performed after automatic irradiation; **c**: MTT assay performed after manual irradiation; **d**: MTT assay performed after automatic irradiation. The Bonferroni test is represented in the graphs and the statistical significance is represented by ▲ if  $p < 0.05$ , ▲▲ if  $p < 0.01$  and ▲▲▲ if  $p < 0.001$ .

**Table 6** indicates the values of the coefficients of variation calculated for each CAP exposure time and technique and the correspondent  $p$  value for the SRB and MTT assays.

First, for 15 seconds, the coefficient of variation is 44.7% for manual CAP irradiation and 19.7% for the automatic CAP irradiation, with  $p = 0.006$ .

For 30, 60, 90 and 120 seconds, **Table 6** shows that the coefficient of variation is smaller for the CAP irradiation with the robotic system, although, as  $p > 0.05$ , the result is not statistically significant.

As discussed for **Figure 31**, the variability of results for the CAP irradiation with the robotic system seems to be smaller than when the technique is performed manually, and this hypothesis is supported by the results in **Table 6**.

For 15 seconds of CAP irradiation time, the coefficient of variation of the results is 49.6% for the results corresponding to the manual CAP application, and 14.5% for the results corresponding to the robotized CAP application, with  $p$  statistically significant. So, these results support the hypothesis that the use of the robotic system reduces the variability of the results.

The values obtained for the coefficient of variation corresponding to manual and robotized CAP application, are, respectively, 85.3% and 42.8%, with  $p < 0.05$ .

Then, for 60 and 90 seconds, the coefficient of variation is bigger for the manual CAP irradiation, and for 120 seconds, the coefficient is bigger for the robotized CAP application, however,  $p > 0.05$ .

**Table 6** - Coefficients of variation for manual and automatic technique of CAP application for ECC-1 cell line for SRB and MTT assay, n.s. (not significant).

Assay	Time (s)	Manual CAP irradiation (%)	CAP irradiation using the robotic system (%)	<i>p</i>
SRB	15	44.7%	19.7%	<b>0.006</b>
	30	53.3%	38.5%	n.s.
	60	73.9%	63.0%	n.s.
	90	59.2%	50.0%	n.s.
	120	55.8%	41.2%	n.s.
	Overall	63.4%	67.3%	n.s.
MTT	15	49.6%	14.5%	<b>0.008</b>
	30	85.3%	42.8%	<b>0.047</b>
	60	156.2%	93.9%	n.s.
	90	96.4%	57.1%	n.s.
	120	63.3%	131.8%	n.s.
	Overall	124.0%	119.0%	n.s.

Generically, the variability of the results (the size of the interquartile range) corresponding to the manual application of CAP, appears to be larger than the results corresponding to the automatic application of CAP. The results demonstrate that, with the use of the robotic system, the variability shows a tendency to decrease. Considering that the only difference in all the procedures was the technique of application of CAP, the difference in the variability can be linked to this factor.

For the RL-95 cell line, the results obtained for the metabolic activity and protein content, which are directly related with cell viability, were plotted with the same presentation as for ECC-1, mentioned above.

The results of protein content are presented in the graphs of **Figure 32-a** and **Figure 32-b**, corresponding to the manual and robotized CAP application, respectively.

For 15 seconds of CAP irradiation time, in the graph of **Figure 32-a**, corresponding to manual CAP irradiation, the interquartile range of the boxplot goes from, approximately, a value of 20 to 50% of protein content, and, for the same CAP irradiation time, when the CAP irradiation is performed with the robotic system, the

interquartile range of the boxplot varies from, approximately, 20 to 40% of protein content.

For CAP irradiation of 30 seconds, for the manual CAP application, the variability of the boxplot is from, approximately, 17 to 45% of protein content, whereas, in the case of application with the robotic system, the variability of the boxplot is in a range that varies from, approximately, 15 to 25% of protein content.

Then, for the time irradiation of 60 seconds, while the boxplot corresponding to the manual CAP irradiation presents an interquartile range from 20 to 50% of protein content, the boxplot corresponding to automatic CAP irradiation presents an interquartile range from, approximately, 15 to 30% of protein content.

For the irradiation time of 90 seconds, the boxplot corresponding to the manual CAP application presents an interquartile range that varies approximately between 15 and 45% of protein content, and the boxplot corresponding to the CAP application with the robotic system presents an interquartile range distribution from 10 to 30% of protein content, approximately. Lastly, for 120 seconds of CAP irradiation time, the boxplot corresponding to manual CAP irradiation presents an interquartile range with values between 10 and 50% of protein content, approximately, whereas the boxplot from the irradiation with the robotic system presents a dispersion between, approximately, 15 and 25% of protein content.

In general, regarding the protein content results, illustrated in the graphs of **Figure 32-a** and **Figure 32-b**, it can be observed that the interquartile range of the boxplots of both graphs always intersect for the same irradiation time. This is important to prove that the use of the robotic system to perform the CAP irradiation does not appear to interfere with the tendency of the results of protein content.

The same interpretation made for protein content can be applied to the analysis of the results of the metabolic activity, for RL-95 cell line.

**Figure 32-c** presents the illustration of results of metabolic activity for the manual CAP irradiation, while **Figure 32-d** refers to the illustration of results of the metabolic activity when CAP irradiation was performed with the robotic system.

In the case of the irradiation time of 15 seconds, the boxplot corresponding to the manual CAP irradiation, illustrated in **Figure 32-c**, presents a variability from 5 to 20% of metabolic activity, approximately, and the boxplot corresponding to the CAP

irradiation with the robotic system, illustrated in **Figure 32-d**, presents a variability with a range from, approximately, 10 to 20% of metabolic activity.

Then, for 30 seconds of CAP irradiation time, for the manual CAP irradiation, the interquartile range of the boxplot varies from 0 to 20% of metabolic activity, approximately. For the results corresponding to the irradiation with the robotic system, the interquartile range of the boxplot varies from 5 to 10% of metabolic activity, approximately.

For 60 seconds of CAP irradiation time, the boxplot corresponding to manual CAP irradiation presents an interquartile range between 0 and 10% of metabolic activity, approximately, and for the case of CAP irradiation with the robotic system, the interquartile range of the boxplot is distributed between, approximately, 0 and 7% of metabolic activity.

For CAP irradiation time of 90 seconds, the results corresponding to the manual CAP irradiation vary from 0 to 12% of metabolic activity, approximately, and the results corresponding to the robotized CAP irradiation vary from 0 to 5% of metabolic activity.

Lastly, for 120 seconds of irradiation time, the variability of the boxplot corresponding to manual CAP irradiation varies from 3 to 5% of metabolic activity, approximately, and is slightly smaller than the variability of the boxplot corresponding to the robotized CAP application, which varies from 0 to 5% of metabolic activity, approximately.

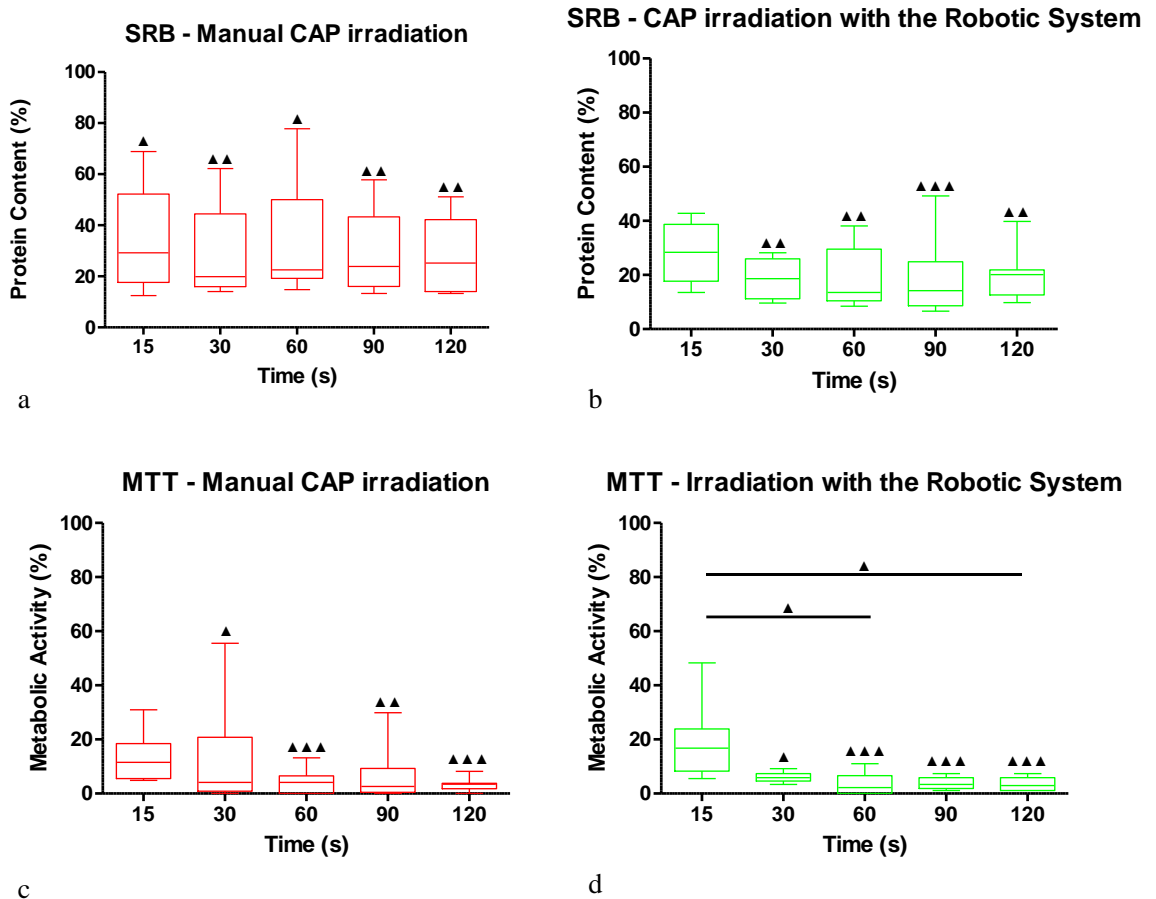


**Figure 32** - Boxplots of the results of the viability assays performed after RL-95 cell line CAP irradiation. **a**: SRB assay performed after manual irradiation; **b**: SRB assay performed after automatic irradiation; **c**: MTT assay performed after manual irradiation; **d**: MTT assay performed after automatic irradiation. The Bonferroni test is represented in the graphs and the statistical significance is represented by ▲ if  $p < 0.05$ , ▲▲ if  $p < 0.01$  and ▲▲▲ if  $p < 0.001$ .

In the case of the studies in RL-95 cells, all the metabolic activity and protein content results show that the interquartile ranges of the boxplots intersect in the range, supporting the idea that the technique of CAP application using the robotic system does not influence the tendency of the metabolic activity and protein content results, so, does not influence CAP treatment in cells. Furthermore, in general, the dispersion of results is smaller when the technique of application of CAP is performed with the robotic system, suggesting that the robotic system performs the technique in a more coherent manner.

**Table 7** displays the coefficient of variation between manual and robotized CAP application in RL-95, for each time interval, for the SRB and MTT assays.

With the analysis of **Table 7**, it can be verified that, in spite of the results not being statistically significant ( $p > 0.05$ ) for protein content, the values of the coefficient of variation are bigger for the case of manual CAP application than for the automatic CAP application, with the exception of 90 seconds of CAP exposure.

These values suggest that the use of the robotic system reduces the variability and increases the precision of the results.

Concerning the metabolic activity, for 30 seconds of CAP exposure time, the value of the coefficient of variation corresponding to the results of manual CAP irradiation is 138.5%, while for the results corresponding to the robotized CAP irradiation is 30.5%, with  $p < 0.05$ . This represents a big difference in the dispersion.

The values of the coefficient of variation, for 15 and 120 seconds, are substantially smaller for the manual CAP irradiation, however, as  $p > 0.05$ , the result is not statistically significant. Thus, it would be advisable to perform more assays. Despite these two results, both for 60 and 90 seconds of CAP irradiation, the coefficient shows a potential to be higher for robotized CAP application.



**Table 7** - Coefficients of variation for manual and automatic technique of CAP application for RL-95 cell line for SRB and MTT assay, n.s. (not significant).

Assay	Time (s)	Manual CAP irradiation (%)	CAP irradiation using the robotic system (%)	<i>p</i>
<b>SRB</b>	15	55.3%	38.4%	n.s.
	30	60.3%	37.6%	n.s.
	60	62.5%	56.8%	n.s.
	90	54.9%	75.2%	n.s.
	120	52.4%	47.0%	n.s.
	Overall	55.9%	51.6%	n.s.
<b>MTT</b>	15	65.4%	67.7%	n.s.
	30	138.5%	30.5%	<b>0.034</b>
	60	109.4%	103.3%	n.s.
	90	148.9%	60.6%	n.s.
	120	74.0%	75.1%	n.s.
	Overall	134.2%	118.1%	n.s.

Hela cell line was the third cell line used for the study, and the results of the metabolic activity and protein content for this, after CAP treatment, are shown in the graphs of **Figure 33**, to support the further discussion.

For the shorter CAP irradiation time – 15 seconds –, manual CAP irradiation has, in **Figure 33-a**, an interquartile range varying from, approximately, 15 to 75% of protein content, whereas, the robotic system, illustrated in **Figure 33-b**, presents interquartile ranges from, approximately, 75 to 95% of protein content.

Then, for 30 seconds of irradiation time, manual CAP irradiation refers to a boxplot with an interquartile range from, approximately, 15 to 60% of protein content, while the boxplot resultant from irradiation with the robotic system presents an interquartile range from, approximately, 70 to 90% of protein content.

For 60 seconds of CAP irradiation time, the boxplot corresponding to manual CAP irradiation shows an interquartile range that varies between, approximately, 10 to 30% of protein content, and the boxplot corresponding to the irradiation with the robotic system presents an interquartile range from 45 to 60% of protein content.

For 90 seconds of CAP irradiation, the boxplot of the manual CAP application, illustrated in the graph of **Figure 33-a**, has an interquartile range that varies from, approximately, 5 to 30% of protein content, and, for the case of automatic CAP application, illustrated in the graph of **Figure 33-b**, the interquartile range of the boxplot varies from, approximately, 25 to 35% of protein content.

For the time of 120 seconds, the results corresponding to the manual CAP application present a boxplot with a dispersion from, approximately, 10 to 30% of protein content, and results corresponding to the robotized CAP application present a boxplot with a dispersion from, approximately, 15 to 20% of protein content.

The metabolic activity results are illustrated in the graphs of **Figure 33-c** and **Figure 33-d**, considering manual and robotized CAP application, respectively.

For 15 seconds of CAP irradiation, the values of metabolic activity corresponding to the manual CAP irradiation present a boxplot with an interquartile range from, approximately, 30 to 75%, whereas the boxplot corresponding to the automatic CAP application displays an interquartile range from, approximately, 40 to 95%.

For 30 seconds of CAP irradiation, the boxplot corresponding to the manual process presents an interquartile range varying from, approximately, 35 to 90 % of metabolic activity, and the boxplot that presents the results corresponding to the irradiation performed with the robotic system shows a boxplot with an interquartile range varying between 10 and 60% of metabolic activity, approximately.

Following, for 60 seconds of CAP irradiation time, the results corresponding to the manual CAP application present a boxplot with a dispersion between the values 5 and 45% of metabolic activity, approximately, and the results corresponding to the robotized CAP application show a boxplot with a dispersion from 5 to 40% of metabolic activity.

Then, as it can be seen, after 90 seconds CAP irradiation time, the variability of the boxplot corresponding to the manual CAP irradiation goes from 0 to 10% of metabolic activity, while the variability of the boxplot corresponding to the robotized CAP application varies between 5 and 10% of metabolic activity, approximately. For last, the CAP irradiation time of 120 seconds presents a boxplot with an interquartile range from, approximately, 0 to 8% of metabolic activity, considering manual CAP

application. For the boxplot corresponding to the robotized CAP application, the interquartile range varies between, approximately, 5 to 8% of metabolic activity.

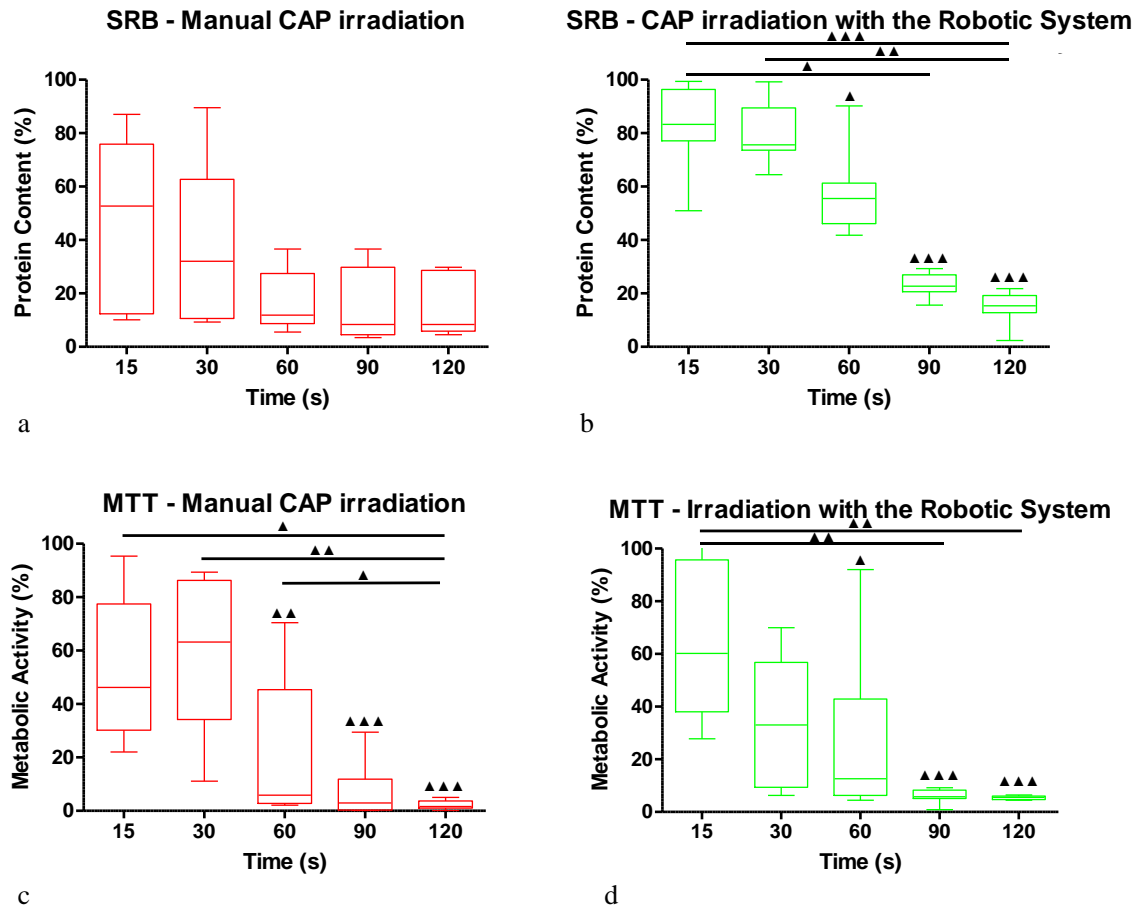


**Figure 33** - Boxplots of the results of the viability assays performed after Hela cell line CAP irradiation. **a**: SRB assay performed after manual irradiation; **b**: SRB assay performed after automatic irradiation; **c**: MTT assay performed after manual irradiation; **d**: MTT assay performed after automatic irradiation. The Bonferroni test is represented in the graphs and the statistical significance is represented by ▲ if  $p < 0.05$ , ▲▲ if  $p < 0.01$  and ▲▲▲ if  $p < 0.001$ .

Analysing the obtained results for protein content (**Figure 33-a** and **Figure 33-b**), for 60 seconds of CAP exposure, the ranges from the minimum to the maximum values of the boxplots, concerning manual and robotized CAP application, do not intersect at any point. This significant difference in the results is difficult to understand, but a possible explanation could be the fact that, when the CAP irradiation was manually performed, the irradiation time can have been counted without rigor and the electrodes were left to irradiate CAP in the cells for more time than what was supposed. This because, for 15, 30 and 60 seconds of CAP irradiation time, the interquartile ranges of

the boxplots considering manual CAP application is, generically, much larger than the interquartile ranges of the boxplots considering robotized CAP application.

For 90 and 120 seconds of CAP irradiation, the interquartile ranges of the boxplots of both figures intersect, with the means of the results corresponding to the manual CAP irradiation presenting lower values.

In general, it can be observed that, in the metabolic activity results, for all of the CAP irradiation times, considering both manual and robotized CAP application, the dispersion of the results, visually represented by the interquartile ranges of the boxes of the boxplots, intersects partially or completely for all the times tested, and it is smaller for results considering robotized CAP application, time intervals. In this way, the dispersion of the results appears to demonstrate a potential to be smaller when the technique used for CAP application is the robotic system, and the tendency of the metabolic activity results are similar with manual and automatic CAP application.

**Table 8** presents the coefficient of variation of the results of protein content and metabolic activity between manual and automatic CAP application, in Hela cells.

All the exposure times refer to statistically significant results, with  $p < 0.05$ . So, the use of the robotic system reduces the variability and increases significantly the precision of the results.

Considering the metabolic activity, it can be seen that the coefficient of variation, for 90 seconds of CAP exposure, is 136.0% and 40.9% ( $p < 0.05$ ), concerning manual and robotized CAP application, respectively. For 120 seconds of CAP exposure, the coefficient of variation is, also, significantly bigger considering robotized CAP application, 73.3%, while considering manual CAP application, the coefficient assumes a value of 12.9%.

**Table 8** - Coefficients of variation for manual and automatic technique of CAP application for HeLa cell line for SRB and MTT assay, n.s. (not significant).

Assay	Time (s)	Manual CAP irradiation (%)	CAP irradiation using the robotic system (%)	<i>p</i>
<b>SRB</b>	15	64.4%	18.0%	<b>0.001</b>
	30	80.4%	13.7%	<b>0.003</b>
	60	64.3%	24.9%	<b>0.006</b>
	90	90.0%	18.3%	<b>&lt;0.001</b>
	120	76.6%	38.3%	<b>0.000</b>
	Overall	93.5%	58.8%	<b>&lt;0.001</b>
<b>MTT</b>	15	47.6	44.0	n.s.
	30	49.3	67.7	n.s.
	60	113.3	122.1	n.s.
	90	136.0	40.9	<b>0.034</b>
	120	73.3	12.9	<b>0.001</b>
	Overall	107.8	110.9	n.s.

All the results achieved for the three cell lines show that the visible difference between the results obtained with manual and automatic CAP application is the variability. The results obtained with the manual application of CAP are, in general, more disperse than the results obtained when the CAP irradiation is performed with the robotic system. This difference in the variability can also be a consequence of the fact that, when operating the CAP irradiation manually, the researcher is also counting the irradiation time, which may result in possible errors.

Summing up, evaluating all the results obtained, the robotic system demonstrates a potential to reduce the variability and increase the precision.

## 6.2.2 BIOLOGICAL SIGNIFICANCE

### 6.2.2.1 ECC-1

CAP potential in cancer treatment and its consequences and effects are still very far from being completely understood.

In ECC-1 cells (**Figure 31-b and Figure 31-d**), from a biological point of view, the results obtained after robotized CAP application showed a decrease of protein content in response to the increase of time exposure to CAP.

For CAP exposure time of 30 seconds, the protein content decreased to  $45.63 \pm 0.01\%$  ( $p < 0.01$ ). Then, for 60 seconds of CAP irradiation time, the values of protein content decreased to  $35.14 \pm 0.01\%$  ( $p < 0.01$ ).

With the time interval increased to 90 seconds, protein content decreased to  $20.66 \pm 0.01\%$  ( $p < 0.001$ ), and for 120 seconds of CAP exposure, to  $14.61 \pm 0.01\%$  ( $p < 0.001$ ).

The metabolic activity results also presented a decrease, with the increase of CAP irradiation time. In fact, the values of metabolic activity decreased to  $7.81 \pm 0.01\%$  ( $p < 0.001$ ), to  $4.22 \pm 0.01\%$  ( $p < 0.001$ ) and to  $3.93 \pm 0.01\%$  ( $p < 0.001$ ) after 60, 90 and 120 seconds of CAP exposure, respectively.

These results demonstrate that the decrease in metabolic activity and in protein content is, in general, significant, which is translated into a decrease in cell viability related to the increase of time exposure to CAP. This suggests that CAP has, indeed, potential to kill tumor cell lines, which depends on time.

ECC-1 cell line seems to have a significant sensibility to CAP treatment from 60 to 120 seconds of exposure and beyond, since it is where the viability is lower.

### 6.2.2.2 RL-95

From the biological point of view, and considering the protein content results for robotized CAP application (**Figure 32-b**), the obtained values were  $18.79 \pm 0.01\%$  ( $p < 0.01$ ),  $19.13 \pm 0.01\%$  ( $p < 0.01$ ),  $18.05 \pm 0.01\%$  ( $p < 0.001$ ) and  $19.20 \pm 0.01\%$  ( $p < 0.01$ ) for 30, 60, 90 and 120 seconds of irradiation, respectively.

As it can be seen, the tendency of protein content is to decrease notably in response to CAP treatment of 15 seconds. For the following times, the values of protein content are similar, which suggests that RL-95 is sensible to CAP treatment for reduced time irradiations.

Considering the metabolic activity results, similarly to protein content, an accentuated decrease for the first CAP irradiation time was verified and, then, the results remained low for the other tested CAP irradiation times.

The values of the metabolic activity, represented in the graph of **Figure 32-d**, decreased to  $6.14 \pm 0.01\%$  ( $p < 0.05$ ), to  $3.79 \pm 0.01\%$  ( $p < 0.001$ ), to  $3.76 \pm 0.01\%$  ( $p < 0.001$ ) and to  $3.39 \pm 0.01\%$  ( $p < 0.001$ ) for 30, 60, 90 and 120 seconds of CAP exposure, respectively. Thus, the values were similar among the CAP exposure times tested.

For RL-95 cell line, an abrupt decrease in protein content and metabolic activity was verified between the control and the shorter CAP irradiation time, 15 seconds. For all the longer irradiation times, the differences in protein content were not significant and the values remained all under 30%. Therefore, CAP appears to have potential to kill tumor RL-95 cells, with small irradiation time intervals.

These results, compared with the results obtained for ECC-1 cell line, suggest that endometrial tumor cell lines present different behaviours, when exposed to CAP treatment.

### 6.2.2.3 HELA

To evaluate the efficacy of CAP in cancer treatment in Hela cell lines, the results of the protein content and metabolic activity associated with cell viability, represented in the graphs of **Figure 33-b** and **Figure 33-d**, are analysed.

Considering robotized CAP application, results show an evident decrease in protein content with the increase in time exposure to CAP. For 60 seconds of CAP treatment, protein content decreased to  $57.44 \pm 0.01\%$  ( $p < 0.05$ ), and for 90 seconds CAP exposure, the value decreased to  $23.17 \pm 0.01\%$  ( $p < 0.001$ ). Then, for 120 seconds of CAP irradiation, the protein content of Hela cells is  $15.01 \pm 0.01\%$  ( $p < 0.001$ ).

These results demonstrate a sensibility of Hela cell lines to CAP treatment, with the protein content decreasing gradually. The cells seem to be more sensitive to CAP from 60 seconds of irradiation and beyond.

Metabolic activity results decreased to  $25.47 \pm 0.01\%$  ( $p < 0.05$ ), to  $6.19 \pm 0.01\%$  ( $p < 0.001$ ) and to  $5.47 \pm 0.01\%$  ( $p < 0.001$ ) for CAP exposure times of 60, 90 and 120 seconds, respectively.

As seen, with the increase in irradiation times, a gradual decrease in metabolic activity and protein content was verified, being significant for 60, 90 and 120 seconds.

Hela cell line appears to demonstrate a higher sensibility to CAP treatment with irradiation times between 60 and 90 seconds, since it is when cell viability shows a larger decrease.

The results of the viability assays showed that CAP induces cell death both in Hela, ECC-1 and RL-95 cells, in a time and cell line dependent way.

The studied cell lines presented different responses to CAP treatment. Specifically, ECC-1 and Hela cell lines verified a bigger sensitivity to high CAP exposure times, above 60 seconds. RL-95 cell line registered a different behaviour, appearing to present a high sensitivity to CAP treatment for lower exposure times (since, for 15 seconds of irradiation time, the cell viability decreased to under 30% of metabolic activity and protein content).



In cancer treatment, it is fundamental to correctly select tumor cells to kill, without damaging adjacent phenotypically normal cells.

In this project, only endometrial tumor cells were studied, so, despite published studies suggesting that CAP presents some selectivity to tumor cells, it would be interesting to proceed this work and investigate the effects of CAP in phenotypically normal cells of endometrium, in order to compare the results and study CAP selectivity. Nevertheless, both the complex plasma composition [63] and the phenotypic differences between normal and tumor cells [64] may be the reason of CAP selectivity [19]. Thus, future work could include a depth study in both fields.

### 6.3 EVALUATION OF THE ROBOTIC SYSTEM

The technique of application of CAP in the cell lines, as it was already mentioned, when performed manually, is a highly time-consuming laboratory task.

During CAP application performed in the present study, the duration of irradiation of each well plate was timed, in order to calculate the average time of CAP irradiation performed manually and with the robotic system. In the accomplished experiments, the time spent in the manual application of CAP in the well plates (all with the conditions mentioned in section 5.2) was, in average, 37 minutes per plate. During this time, the researcher must be highly concentrated and focused exclusively in the practice of this technique, to change the position of the electrodes for each well and calibrate the correct position for the discharge of CAP.

After the development of the robotic system, the average time of application of CAP using this solution decreased to, approximately, 17 minutes, in average. During this time, the researcher does not need to interact with the system, being able to do other useful tasks in the laboratory.

By relating the difference in the irradiation times, it can be estimated the direct reduction of time spent in CAP application in cell lines:

$$\frac{17}{37} \times 100\% \cong 49.95\% .$$

In this way, by replacing the manual system of CAP application by the automatic one, the direct reduction of time in the application of CAP in cell lines is, approximately, 50%. Researchers can save half of the time spent in the laboratory by replacing the system of application of CAP. And, considering that, during CAP irradiation performed by the robotic system, the user can be doing other laboratory tasks, the reduction of time spent with the technique can be much higher, when compared to the time spent performing manual CAP irradiation.

Another important conclusion of this work is that, as it was analysed by **Figure 31**, **Figure 32** and **Figure 33**, the main difference between the results of the viability assays obtained with manual and automatic CAP irradiation was the variability of the measures. The range of the values obtained with automatic CAP irradiation was, generically, smaller than the range of the values resulting from manual irradiation. However, the robotic system appears to not interfere with the CAP influence in cells, since the biological analysis was similar for both techniques. This means that the variability of the results can be reduced by the robotic system, but the values of the results do not present a significant difference between both techniques.

Concluding, the robotic system developed in the present study demonstrated a promising potential to decrease the variability, increasing the precision of the results without influencing CAP mechanisms in cells.



## Chapter 7: Conclusion and Future Work

---

The multidisciplinary nature of this dissertation allowed the synergistic conjugation of the fields of robotics and biology in a complementary project inserted in the area of Biomedical Engineering.

This project proposed the automatization of a laboratory technique: the application of CAP in tumor cell lines. The presented solution enables the user to easily and intuitively customize CAP application in the cells; the application is, then, executed by the system itself.

The achieved results demonstrated that the developed robotic system could autonomously perform the technique successfully. Furthermore, the time of the technique was proven to be directly reduced to half, when compared with the manual practice. In this way, the working time of the researchers in the laboratory becomes more profitable, since, with the robotic system, there is no longer the need to be manually controlling the CAP device.

The present study also suggested that the robotic system has potential to increase the precision of the results without influencing their accuracy.

Future work in the robotic solution could also include the adaptation of the system to more types of well plates, or, even, the adaptation of the automatic system by the increasing of DOF for a possible implementation of *in vivo* studies of tissues or organs of animals in order to implement preclinical studies.

Moreover, this research enlightens the potential of human-robot interaction in medical investigations environment and encourages forthcoming work in automatizing techniques to improve researchers' productivity.

In addition, presented results highlight the potential of CAP in cancer treatment. The assays demonstrated a decrease in the metabolic activity and in the protein content dependent on the exposure time for the three cell lines of the study in different ways.

This dissertation encouraged the understanding and comprehension of CAP treatment potential in endometrial tumor cell lines.

Future work concerning CAP potential in endometrial cancer treatment could include the study of the selective potential of CAP for endometrial tumor cells, comparing with phenotypically normal cells of endometrial tissue. Besides, the identification and classification of the possible mechanisms in the interaction between CAP and tumor cells requires further investigation. It would also be important to study the CAP influence for different tumor cell lines and their exposure times. For high irradiation times, literature has demonstrated that CAP can be fatal not only to tumor cells, but also to phenotypically normal cells, due to the high cytotoxicity, so, this boundary would be interesting to study, too.

CAP may potentially offer a minimally-invasive option that allows specific cell removal without interfering with the whole tissue, which is a great advantage for cancer treatment. For endometrial cancer, it could be useful to study CAP treatment as an adjuvant treatment in TAH-BSO or chemotherapy, evaluating if the synergy of the treatments would be additive or antagonist.



# References

---

- [1] A. D. D. G. S. P. D. S. M. Panteghini, “Total laboratory automation: Do stat tests still matter?,” *Elsevier*, vol. 50, no. 10–11, pp. 605–611, 2017.
- [2] Y. Xiang, J. Tian, Z. Zhang, and Y. Dai, “Diagnosis of endometrial cancer based on back-propagation neural network and near-infrared spectroscopy of tissue,” *6th Int. Conf. Fuzzy Syst. Knowl. Discov. FSKD 2009*, vol. 3, pp. 508–512, 2009.
- [3] S. H. Bendary, E. R. Mostafa, and M. Esmat, “Comparative study between preoperative and operative staging in endometrial cancer patients,” vol. 73, no. October, pp. 7189–7195, 2018.
- [4] S. Kyo, M. Takakura, T. Kohama, and M. Inoue, “Telomerase activity in human endometrium,” *Cancer Res.*, vol. 57, no. 4, pp. 610–614, 1997.
- [5] C. Monteiro, “EGCG DO CHÁ VERDE - UM AGENTE NATURAL CONTRA O CANCRO DA MAMA,” Universidade de Coimbra, 2018.
- [6] Sociedade Portuguesa de Ginecologia, “Cancro Ginecológico,” *Consensos Nac. 2016*, pp. 1–167, 2016.
- [7] F. Mota, “22 Cancro do endométrio,” *Fed. das Soc. Port. Obs. e Ginecol.*, no. m, 2011.
- [8] M. Horta and T. M. Cunha, “Endometrial cancer,” *Med. Radiol.*, vol. 387, no. 10023, pp. 179–208, 2019.
- [9] M. J. da S. F. L. Carvalho, “Células estaminais do cancro do endométrio. Caracterização, resposta à terapêutica e padrão de metastização in vivo,” 2015.
- [10] S. B. Edge, D. R. Byrd, C. C. Compton, A. G. Fritz, F. L. Greene, and A. Trotti III, *7th ed 2010 AJCC Cancer Staging Manual Seventh Edition*. 2010.
- [11] J. C. KUMAR, Vinay; ABBAS, Abul K.; ASTER, *Kumar - Robbins Patologia Básica*, 9th ed. 2013.
- [12] I. V. Frederic Amant, Philippe Moerman, Patrick Neven, Dirk Timmerman, Erik Van Limbergen, “Endometrial Cancer,” *ScienceDirect*, 2005.
- [13] U. M. Haltia, R. Bützow, A. Leminen, and M. Loukovaara, “FIGO 1988 versus 2009 staging for endometrial carcinoma: A comparative study on prediction of survival and stage distribution according to histologic subtype,” *J. Gynecol. Oncol.*, vol. 25, no. 1, pp. 30–35, 2014.
- [14] V. S. BS Sunita, Arijit Sen, “To evaluate immunoreactivity of cyclooxygenase-2 in cases of endometrial carcinoma and correlate it with expression of p53 and vascular endothelial growth factor,” 2018.
- [15] “Uterine Cancer: Stages and Grades.” [Online]. Available: <https://www.cancer.net/cancer-types/uterine-cancer/stages-and-grades>. [Accessed: 02-Jun-2019].
- [16] K. C. Wen *et al.*, “Uterine sarcoma Part I—Uterine leiomyosarcoma: The Topic Advisory Group systematic review,” *Taiwan. J. Obstet. Gynecol.*, vol. 55, no. 4, pp. 463–471, 2016.

- [17] Y. Wang and J. X. Yang, “Fertility-preserving treatment in women with early endometrial cancer: The Chinese experience,” *Cancer Manag. Res.*, vol. 10, pp. 6803–6813, 2018.
- [18] M. Steven C Plaxe, S. Editor, M. Barbara Goff, D. Editor, and M. Sandy J Falk, “Endometrial carcinoma: Pretreatment evaluation, staging and surgical treatment,” *Literature review current through: Oct 2013. | This topic last updated: Jan 15, 2013.* [Online]. Available: [http://51.75.30.32/contents/UTD.htm?18/23/18810?source=related\\_link](http://51.75.30.32/contents/UTD.htm?18/23/18810?source=related_link). [Accessed: 05-Aug-2019].
- [19] R. Teixeira, “Targeting cancer with cold atmospheric plasma,” University of Coimbra, 2017.
- [20] W. Li *et al.*, “Cold atmospheric plasma and iron oxide-based magnetic nanoparticles for synergetic lung cancer therapy,” *Free Radic. Biol. Med.*, vol. 130, no. October 2018, pp. 71–81, 2019.
- [21] L. Gan, S. Zhang, D. Poorun, D. Liu, and X. Duan, “Medical applications of nonthermal atmospheric pressure plasma in dermatology,” pp. 1–7, 2017.
- [22] C. Heslin, D. Boehm, V. Milosavljevic, and M. Laycock, “Quantitative Assessment of Blood Coagulation by Cold Atmospheric Plasma,” 2014.
- [23] R. Ozono, “Aplicações biomédicas dos plasmas não térmicos à pressão atmosférica,” pp. 1–17, 2014.
- [24] J. Heinlin *et al.*, “Plasma-Medizin: Anwendungsmöglichkeiten in der Dermatologie,” *JDDG - J. Ger. Soc. Dermatology*, vol. 8, no. 12, pp. 968–977, 2010.
- [25] C. Alexandra and A. Ferreira, “PLASMA FRIO ATMOSFÉRICO COMO ALTERNATIVA TERAPÊUTICA NO CANCRO DA,” 2019.
- [26] A. M. Nokhandani, S. Mahsa, T. Otaghsara, and M. K. Abolfazli, “Review Article A Review of New Method of Cold Plasma in Cancer Treatment,” vol. 3, pp. 222–230, 2015.
- [27] D. Yan, J. H. Sherman, and M. Keidar, “Cold atmospheric plasma , a novel promising anti-cancer treatment modality,” vol. 8, no. 9, pp. 15977–15995, 2017.
- [28] M. Keidar, “Plasma for cancer treatment,” 2015.
- [29] H. Mokhtari, L. Farahmand, K. Yaserian, N. Jalili, and K. Majidzadeh-A, “The antiproliferative effects of cold atmospheric plasma-activated media on different cancer cell lines, the implication of ozone as a possible underlying mechanism,” *J. Cell. Physiol.*, no. August, pp. 1–5, 2018.
- [30] J. F. Kolb *et al.*, “Cold atmospheric pressure air plasma jet for medical applications,” *Appl. Phys. Lett.*, vol. 92, no. 24, pp. 24–27, 2008.
- [31] G. Isbary *et al.*, “issues Cold atmospheric plasma devices for medical issues,” vol. 4440, 2014.
- [32] C. Daniela and C. Rocha, “Sistema de Bancada Laboratorial para Tarefas Repetitivas,” 2016.
- [33] T. Leal, G. Oly, and C. Corleta, “30 Years of Robotic Surgery,” *World J. Surg.*, 2016.



- [34] J.-H. Chen and K.-T. Song, "Collision-Free Motion Planning for Human-Robot Collaborative Safety Under Cartesian Constraint," *2018 IEEE Int. Conf. Robot. Autom.*, pp. 1–7, 2018.
- [35] P. E. Sandin, *Devices Illustrated*, vol. Walkers, no. 4. 2003.
- [36] M. P. Groover, *Automation, Production Systems, and Computer-Integrated Manufacturing*, Third Edit. 2008.
- [37] R. A. Felder, J. C. Boyd, K. Margrey, W. Holman, and J. Savory, "Robotics in the medical laboratory," *Clin. Chem.*, vol. 36, no. 9, pp. 1534–1543, 1990.
- [38] "YASKAWA." [Online]. Available: <https://www.yaskawa.eu.com/en/products/robotics/motoman-robots/productdetail/product/csda10f/>. [Accessed: 14-Mar-2019].
- [39] T. Dahl and M. Boulos, "Robots in Health and Social Care: A Complementary Technology to Home Care and Telehealthcare?," *Robotics*, vol. 3, no. 1, pp. 1–21, 2013.
- [40] S. Jeelani, A. Dany, B. Anand, S. Vandana, T. Maheswaran, and E. Rajkumar, "Robotics and medicine: A scientific rainbow in hospital," *J. Pharm. Bioallied Sci.*, vol. 7, no. 6, p. 381, 2015.
- [41] J. Bodner, H. Wykypiel, G. Wetscher, and T. Schmid, "First experiences with the da Vinci™ operating robot in thoracic surgery," *Eur. J. Cardio-thoracic Surg.*, vol. 25, no. 5, pp. 844–851, 2004.
- [42] J. Q. Gan, "Department of Computer Science TECHNICAL REPORT CSM-413 Forward and Inverse Kinematics Models," no. January 2002, 2015.
- [43] "YASKAWA." [Online]. Available: <https://www.yaskawa.eu.com/en/products/robotics/motoman-robots/productdetail/product/csda10f/>. [Accessed: 01-May-2019].
- [44] "VASCULOGIC." [Online]. Available: <http://www.vasculogic.com/>. [Accessed: 01-May-2019].
- [45] [Online]. Available: [https://gloimg.gbtcdn.com/soa/gb/pdm-product-pic/Distribution/2019/08/15/goods\\_thumb-v13/20190815170553\\_24351.jpg](https://gloimg.gbtcdn.com/soa/gb/pdm-product-pic/Distribution/2019/08/15/goods_thumb-v13/20190815170553_24351.jpg). [Accessed: 13-Dec-2018].
- [46] [Online]. Available: [https://ae01.alicdn.com/kf/HTB1AXntc5AnBKNjSZFvq6yTKXXab/Rob-el-trico-m-dulo-linear-CNC-plataforma-deslizante-el-trico-horizontal-passo-plataforma-de-slides.jpg\\_50x50.jpg](https://ae01.alicdn.com/kf/HTB1AXntc5AnBKNjSZFvq6yTKXXab/Rob-el-trico-m-dulo-linear-CNC-plataforma-deslizante-el-trico-horizontal-passo-plataforma-de-slides.jpg_50x50.jpg). [Accessed: 18-Nov-2018].
- [47] "Autodesk." [Online]. Available: <https://gallery.autodesk.com/projects/anet-a8-3d-printer>. [Accessed: 20-Feb-2018].
- [48] P. M. Matos, "Collaborative Gripper for Robotic Applications Gripper Colaborativo para Aplicações Robóticas," 2019.
- [49] P. Neto, "Off-line programming and simulation from CAD drawings: Robot-assisted sheet metal bending," *IECON Proc. (Industrial Electron. Conf.)*, pp. 4235–4240, 2013.
- [50] "LIFE SCIENCE." [Online]. Available: <https://www.livescience.com/38190-stereolithography.html>. [Accessed: 17-Jun-2019].

- [51] A. Rodríguez-Panes, J. Claver, and A. M. Camacho, “The influence of manufacturing parameters on the mechanical behaviour of PLA and ABS pieces manufactured by FDM: A comparative analysis,” *Materials (Basel)*, vol. 11, no. 8, 2018.
- [52] J. M. G. Valle, J. C. C. Garcia, and E. R. Cadaval, “Electric vehicle monitoring system by using MATLAB/App Designer,” *Proc. - 2017 Int. Young Eng. Forum, YEF-ECE 2017*, pp. 65–68, 2017.
- [53] S. J. Shin, S. H. Suh, and I. Stroud, “Reincarnation of G-code based part programs into STEP-NC for turning applications,” *CAD Comput. Aided Des.*, vol. 39, no. 1, pp. 1–16, 2007.
- [54] T. Welander, “G-code Modeling for 3D Printer Quality Assessment G-code Modeling for 3D Printer Quality Assessment,” 2018.
- [55] D. Soa, “modelagem de serviços com BPMN.”
- [56] E. Team, “Laboratory Info,” *Manual Cell Counting With Neubauer Chamber*, 2019. [Online]. Available: <https://laboratoryinfo.com/manual-cell-counting-neubauer-chamber/>. [Accessed: 10-Aug-2019].
- [57] M. Laranjo, “Fotossensibilizadores para terapia e imagem em oncologia,” p. 266, 2014.
- [58] M. Cândida, B. Mendes, and E. M. Dentária, “MÉTODOS Esterilização Esterilização vs VS adesão VERSUS ADESÃO e ADESÃO proliferação PROLIFERAÇÃO E PROLIFERAÇÃO celular CELULAR EM SCAFFOLDS scaffolds EM SCAFFOLDS para PARA aplicação em EM MEDICINA,” 2017.
- [59] T. L. Riss *et al.*, “Cell Viability Assays,” *Assay Guid. Man.*, pp. 1–31, 2004.
- [60] V. Vichai and K. Kirtikara, “Sulforhodamine B colorimetric assay for cytotoxicity screening,” *Nat. Protoc.*, vol. 1, no. 3, pp. 1112–1116, 2006.
- [61] V. Kuete, O. Karaosmanoğlu, and H. Sivas, “Anticancer Activities of African Medicinal Spices and Vegetables,” *Med. Spices Veg. from Africa Ther. Potential Against Metab. Inflammatory, Infect. Syst. Dis.*, pp. 271–297, 2017.
- [62] “Make me analyst.” [Online]. Available: <http://makemeanalyst.com/explore-your-data-range-interquartile-range-and-box-plot/>. [Accessed: 15-Aug-2019].
- [63] O. Volotskova, T. S. Hawley, M. A. Stepp, and M. Keidar, “Targeting the cancer cell cycle by cold atmospheric plasma,” *Sci. Rep.*, vol. 2, 2012.
- [64] M. Wang, B. Holmes, X. Cheng, W. Zhu, M. Keidar, and L. G. Zhang, “Cold Atmospheric Plasma for Selectively Ablating Metastatic Breast Cancer Cells,” *PLoS One*, vol. 8, no. 9, p. e73741, 2013.